Bimetallic nanoparticles—novel materials for chemical and physical applications†

Naoki Toshima*[,a] and Tetsu Yonezawa[b]

[a] *Department of Materials Sciences and Engineering, Science University of Tokyo in Yamaguchi, Onoda-shi, Yamaguchi 756-0884, Japan*
[b] *Department of Chemistry and Biochemistry, Graduate School of Engineering, Kyushu University, Hakozaki, Fukuoka 812-8581, Japan*

A new class of materials for catalysis have been intensively investigated, that is, 'bimetallic nanoparticles'. Extensive studies of non-supported bimetallic nanoparticle dispersions, stabilized by polymers or ligands, started only about 10 years ago. Many preparative procedures have been proposed, and detailed characterizations have been carried out on bimetallic nanoparticles, thanks to the rapid improvement of analytical technology on surface and nanoscale materials. In this review, we focus on the preparation, characterization and application to catalysis of polymer- or ligand-stabilized bimetallic nanoparticles in dispersion, emphasizing our own work and introducing recent progress of this area.

Contents

1 Introduction

Nanoparticles are currently the subject of intense investigation and research is in progress from a variety of viewpoints.[1–6] Examples include spectroscopic and magnetic properties of quantum size semiconductors,[7–13] synthesis and catalysis of polymer- and ligand-stabilized metal nanoparticles,[14–34] spectroscopic investigations of nanoparticles in the gas phase,[35] examination of ceramics and metals having crystalline regions of only a few nanometers in diameter,[36] photochemistry of semiconductor nanoparticles and non-linear optical properties of metal cluster-doped glasses.[37] Such nanoparticles, defined by a diameter of 1–10 nm, are creating a new category of materials, which is different either from conventional bulk materials or from atoms, the smallest units of matter. This category could be called an 'atom assembly' or 'molecule' rather than using the correct and classical term 'colloid'. If these nanoparticles are well-controlled in structure, the term 'cluster' is now often used. Ligand-stabilized Au_{55} nanoparticles, proposed by Schmid *et al.*,[14] can be considered as one of the most impressive examples of a 'cluster', in which the arrangement of metal atoms as well as ligand molecules can be specified. In the case of polymer-stabilized metal nanoparticles, the structure and arrangement of the polymer parts are not known precisely, but those of the metal atoms can be rather precisely analyzed. For these materials we would like to propose the concept of 'inorganic molecule' or 'metal molecule' as the term 'inorganic polymer' is used for materials composed of inorganic units like SiO_2. In any case, there has recently been a vigorous development of the chemistry and physics of nanoparticles, despite the fact that the world of nanoparticles had been neglected by chemists for a long time, probably because of their poly-dispersity or non-uniformity.

Perfectly monodispersed metal nanoparticles are, of course, ideal, but special properties are to be expected even if the ideal is not perfectly realized. Mass production of these nanoparticles with enough uniformity is most important to realize, as most chemical or physical properties of nanosize materials have not been elucidated yet. Much attention is now being paid to this area.

Metal nanoparticles can be prepared by physical and chemical methods. The physical methods, which often involve vapor deposition, consist in principle of subdividing bulk precursors to nanoparticles. Chemical procedures start from reduction of metal ions to metal atoms, followed by controlled aggregation of atoms. From the viewpoint of mass production of metal nanoparticles the chemical method is more important and effective than the physical one.

The most remarkable features of nanoparticles are their specific chemical and physical properties. The effect specific to the small size of nanoparticles is called the 'quantum size effect' (QSE).[38] This effect has been theoretically established by a Japanese physicist, Kubo.[39] Another kind of special property of nanoparticles is caused by the fact that a high ratio of atoms are located on the surface in nanoparticles. In other words, the number of atoms at the surfaces or grain boundaries of nanoparticles is comparable to or even bigger than the number that are located in the bulk core. A typical example of these special properties is observed in NMR spectra of metal nanoparticles. For example, ^{195}Pt NMR spectra of 0.7–1.2 nm Pt nanoparticles have a broad peak because of the quantum effect of free electrons.[40–43] That is, some Pt atoms show the spectrum corresponding to those in the metallic state and others in the same nanoparticle show that of somewhat oxidized states. It has recently become possible to measure many special physical properties, like the NMR spectra, thanks to the mass production of 'adequately monodispersed' nanoparticles by chemical methods.

Among the chemical properties of metal nanoparticles, catalysis is of great interest and is the best investigated.[3,4,18,44–58] The particle size can affect not only the activity but also the selectivity of catalysts.

Bimetallic nanoparticles, composed of two different metal elements, are of greater interest than monometallic ones, from both the scientific and technological views, for the improvement of the catalytic properties of metal particles.[59–61] This is because bimetallization can improve catalytic properties of the original single-metal catalysts and create a new property, which may not be achieved by monometallic catalysts. These effects of the added metal component can often be explained in terms of an ensemble and/or a ligand effect in catalyses.

Sinfelt and coworkers have vigorously studied inorganic oxide-supported bimetallic nanoparticles for catalysis and analyzed their micro-structures by an EXAFS technique.[60,62–64] These supported bimetallic nanoparticles have already been used as effective catalysts for the hydrogenation of olefins and carbon-skeleton rearrangement of hydrocarbons. The alloy structure can be carefully examined to understand their catalytic properties.

In contrast, colloidal dispersions of bimetallic nanoparticles have not been well-examined until recently. Metal nanoparticles without inorganic supports may have some advantages in comparison with the supported ones. For example, the intrinsic properties of metal nanoparticles can be elucidated without the effect of the metal–support interaction. In addition, more uniform particle sizes can be obtained in the dispersed systems than in the supported cases, especially under conditions of high metal concentration, because the dispersed metal nanoparticles can be easily concentrated by evaporating the solvent without changing the structures; in contrast the higher loading of metal on inorganic supports normally gives bigger particles with wider particle size dispersions.

In this article, we will focus on colloidal dispersions of bimetallic nanoparticles prepared by chemical methods. After surveying the preparation procedures, details of characterization methods and examples will be discussed with emphasis on our own work. The application of bimetallic nanoparticles to catalysis will follow, and in closing other aspects will be mentioned briefly.

2 Preparation of Colloidal Dispersions of Monometallic and Bimetallic Nanoparticles

2.1 Monometallic nanoparticles

Metal nanoparticles can be prepared by two distinct ways, that is, by subdivision of bulk metals (a physical method) and by the growth of particles starting from metal atoms, which are obtained from molecular or ionic precursors (a chemical method) (Fig. 1). The latter preparative method is more suitable to obtain small and uniform nanoparticles than the former. In the latter method, control of the atom aggregation is the most important step to control the size and uniformity of the metal nanoparticles.

Since the days of Michael Faraday, who first scientifically elucidated the preparative method for aqueous dispersions of metal nanoparticles,[65] metal nanoparticles have often been produced by chemical reduction of the corresponding metal salts in solution in the presence of suitable stabilizers.[66] Faraday's Au nanoparticle dispersions can be considered to be dispersed without any stabilizer, but, in fact, citrate ions, which are the reductants of Au^{III} ions to Au^0 atoms, are adsorbed on the surface of Au nanoparticles and stabilize them by an electrostatic repulsive force. Thus, the citrate ions reduce Au^{III} ions, control the growth of Au atoms to metal nanoparticles, and stabilize the obtained Au nanoparticles.

In a second stage, Nord and Turkevich have carried out extensive studies and introduced metal nanoparticles as effective catalysts. Faraday found that the addition of gelatin to

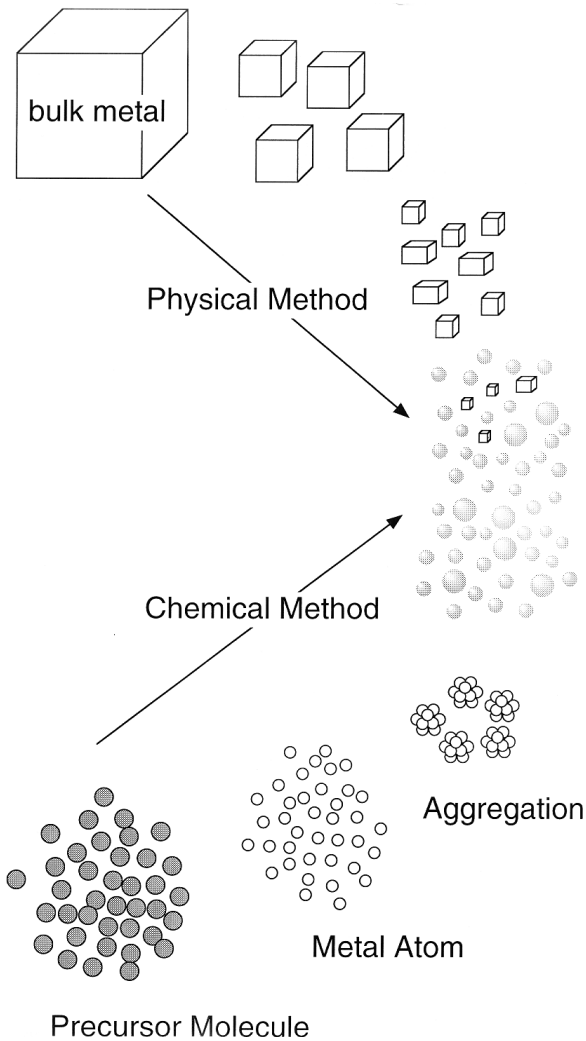

Fig. 1 Schematic illustration of preparative methods of metal nanoparticles

gold sols protected them from the action of salts. Nord and coworkers advanced this idea and used synthetic polymers, such as poly(vinyl alcohol), as a protective colloid for Pd or Pt nanoparticles and applied them to catalysts.[44–47] Turkevich and colleagues introduced Pd,[67] Pt [68] and Au [69] nanoparticles, produced by citrate reduction, for use as supported catalysts.

Ligands or polymers, especially solvent-soluble polymers, either natural or synthetic, with some affinity for metals are often used as stabilizers of metal nanoparticles.[1,48,70–72] These substances also control both the reduction rate of metal ions and the aggregation process of metal atoms. Preparation of polymer-stabilized nanoparticles by a chemical method involves two processes: reduction of metal ions to zerovalent atoms and coordination of the stabilizing polymer to metal nanoparticles.

Polymers also control the aggregation process of metal atoms in solution. In practice, reduction can be preceded or followed by the interaction between metallic species and polymers. If the reduction precedes the interaction, the structural properties of metal nanoparticles are determined only by the reduction conditions. However, if the interaction precedes the reduction, the interactive forces between polymers and metal ions may affect the size and structure of metal nanoparticles. Fig. 2 illustrates the latter process. If the polymer–metal interaction precedes the reduction, a 'complex' of metal ions with a stabilizing polymer is formed first ('polymer–metal *ion* complex'), followed by the reduction of metal ions under mild conditions. Subsequently, the metal atoms thus produced maintain an interaction with the stabilizing polymer ('polymer–metal *atom* complex'). However, if the reduction precedes the interaction, complex formation between polymers and metal ions may not occur, and the growth of metal atoms may not be well-controlled by stabilizing polymers.

Fig. 3 illustrates a typical stabilization structure of a metal nanoparticle by soluble polymers in an aqueous solution. Stabilizing polymers, both natural and synthetic, can be adsorbed on the surface of hydrophobic metal nanoparticles. Hydrophobic 'train' segments are directly adsorbed on the surface of solid metal, and hydrophilic 'loop' or 'tail' segments spread out into the hydrophilic solvent. This stabilization mechanism has been discussed as steric stabilization. The strong adsorption of stabilizing polymers on metal nanoparticle surfaces is usually explained on the basis of adsorption isotherm data.

Our group has invented a so-called 'alcohol-reduction' process to prepare the colloidal dispersions of small and uniform metal nanoparticles.[48,49,73,74] Refluxing of alcohol solutions of metal ions in the presence of a protective polymer gives homogeneous colloidal dispersions of the corresponding metal nanoparticles. Alcohols, such as ethanol, methanol, 2-propanol, glycol, or ethoxyethanol, work as a solvent as well

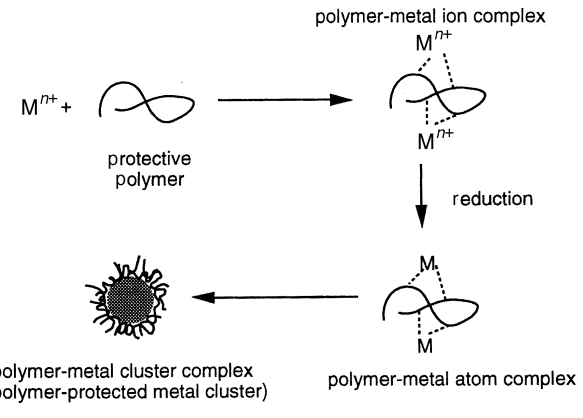

Fig. 2 Schematic illustration of the reduction process of metal salts in the presence of a stabilizing polymer

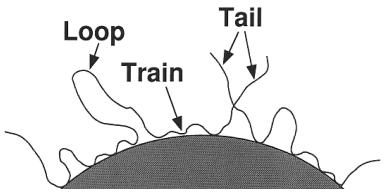

Fig. 3 Schematic illustration of the stabilizing structure of polymers on the surface of metal nanoparticles

as a reductant, being oxidized into aldehydes or ketones. This preparative method has the following advantages. (*i*) The procedure is very simple and reproducible. (*ii*) Particle size of the obtained metal nanoparticles is small with a narrow size distribution. (*iii*) The particle size can be controlled by altering the preparative conditions, such as the choice of alcohol, reducing temperature, quantity and variety of stabilizing polymers, concentration of metal ions and additives, and so forth. (*iv*) The obtained colloidal dispersions of metal nanoparticles show a high catalytic activity. (*v*) The obtained colloidal dispersions are stable and no precipitates are observed for years. In Table 1, a variety of preparative conditions and the results are listed.[49,71,74] Almost all precious metal nanoparticles can be prepared by this alcohol-reduction method.

The classical Faraday citrate sol can be regarded as the oldest ligand-stabilized nanoparticle, even though no traditional ligand was contained and the size distribution was very wide. Recently, however, the preparation of ligand-stabilized metal nanoparticles has been proposed on the basis of organometallic chemistry.[14,75,76]

Organic ligands with a group having an affinity for metals, like a phosphine group (≡P),[14,76] are often used to stabilize metal nanoparticles. For Au nanoparticles, thiol derivatives (—SH) have been recently used as strong stabilizers.[26,30,32] Thiol derivatives are also used to functionalize the Au surface by formation of a monolayer on the surface with strong coordination.

The most famous ligand-stabilized metal nanoparticle is probably $Au_{55}(PPh_3)_9$, prepared by Schmid *et al.*[14] Careful addition of diborane into an Au^{III} ion solution in the presence of PPh_3, followed by column separation, gives small and quite uniform Au nanoparticles, most of them having a Au_{55} structure.

Citrate reduction of Au^{III} ion with the addition of water-soluble thiol ligands[32] and borohydride reduction of Au^{III} ion in the presence of thiol ligands[26,30] also give uniform Au

Table 1 Preparation of colloidal dispersions of precious metal nanoparticles by reduction of the corresponding metal ions with alcohol in the presence of polymer[a]

	Preparative conditions		
Metal salt	In alcohol[b]	With water[c]	With base[d]
$RuCl_3 \cdot 3H_2O$	−	+	−
$RhCl_3 \cdot 3H_2O$[49]	+	+	+
$PdCl_2 \cdot 3H_2O$[71]	+	+	+
$AgNO_3$	+	−	+
OsO_4[74]	+	+	+
Na_2IrCl_6[74]	+	+	+
$H_2PtCl_6 \cdot 6H_2O$	−	+	+
$HAuCl_4 \cdot 4H_2O$	−	+	+

[a] The stability of the colloidal dispersions is shown as + (stable) or − (unstable). [b] Refluxing in anhydrous ethanol in the presence of poly(*N*-vinyl-2-pyrrolidone). [c] Refluxing in methanol–water in the presence of poly(*N*-vinyl-2-pyrrolidone). [d] Refluxing in methanol in the presence of poly(*N*-vinyl-2-pyrrolidone) and then on addition of NaOH.

nanoparticles. Their advantage is that the Au–thiol ligand ratio controls the size of the Au nanoparticles with a narrow size distribution.[26,32]

2.2 Bimetallic nanoparticles

Metal nanoparticle catalysts composed of two (or more) different metal elements are of interest from both technological and scientific views for improving the catalyst quality or properties.[59] In fact, bimetallic (or multimetallic) catalysts have long been valuable for in-depth investigations of the relationship between catalytic activity and catalyst particle structure.[60]

Sinfelt *et al.* have made a series of studies on bimetallic nanoparticle catalysts supported on inorganic supports, for example Ru–Cu[77] and Pt–Ir[78] on silica. They analyzed the detailed structure of their samples by an extended X-ray absorption fine structure (EXAFS) technique, and showed that these nanoparticles with a diameter of 1–3 nm had an alloy structure, associated with their special properties.[62–64,77–79]

Preparation of bimetallic nanoparticles from metal salts can be divided into two groups; co-reduction and successive reduction of two metal salts. Co-reduction is the most simple preparative method of bimetallic nanoparticles, that is, the same as that of monometallic nanoparticles. The only difference is the number of metal precursors. Successive reduction is usually carried out to prepare 'core–shell' structured bimetallic nanoparticles. Other methods, such as preparation from double complexes and electrolysis of bulk metal, will be reviewed too.

2.2.1 Co-reduction of mixed ions. Au–Pt bimetallic nanoparticles were prepared by citrate reduction by Miner *et al.* from the corresponding two metal salts, such as tetrachloroauric(III) acid and hexachloroplatinic(IV) acid.[80] Reduction of the metal ions is completed within 4 h after the addition of citrate. In Fig. 4, UV/VIS spectra of citrate-stabilized Au–Pt bimetallic nanoparticles are collected. The spectrum of the bimetallic nanoparticles is not a simple sum of those of the two monometallic nanoparticles, indicating that these bimetallic nanoparticles have an alloy structure. The average diameter of the bimetallic nanoparticles depends on the metal composition. By a similar method, citrate-stabilized Pd–Pt bimetallic nanoparticles can also be prepared.[80]

Polymer-stabilized bimetallic nanoparticles in water–alcohol have been prepared by simultaneous reduction of the two corresponding metal ions with refluxing alcohol. For example, colloidal dispersions of Pd–Pt bimetallic nanoparticles can be prepared by refluxing the alcohol–water (1 : 1 v/v) mixed solution of palladium(II) chloride and hexachloroplatinic(IV) acid in the presence of poly(*N*-vinyl-2-pyrrolidone) (PVP) at about 90–95 °C for 1 h.[81–83] The resulting brownish colloidal dispersions are stable and neither precipitate nor flocculate over a period of several years.

Richard *et al.* succeeded in preparing Pt–Ru bimetallic nanoparticles by co-reduction of the corresponding metal salts in the presence of glucose.[84] EXAFS data indicated the existence of a Pt—Ru bond in this case, proving the formation of bimetallic nanoparticles. Pd–Rh bimetallic nanoparticles, stabilized by PVP, were also prepared by the alcohol reduction process.[85]

Nanoparticles of the light transition metals are more difficult to prepare because of the lower redox potentials of the corresponding metal ions compared to those of the precious metal ions. In other words, light transition metal ions are difficult to reduce and zerovalent light transition metals are easily oxidized. However, these light transition metals are very important materials for catalysis and other applications, such as magnetic materials.

Polymer-stabilized bimetallic nanoparticles containing both a light transition metal element and a precious metal element can also be prepared by a modified alcohol reduction procedure. For example, Cu–Pd bimetallic nanoparticles were successfully prepared with various Cu : Pd ratios by refluxing a glycol solution of the hydroxides of Cu and Pd in the presence of PVP or by thermal decomposition of metal acetates. Either method needs solvents with high boiling points (ethylene glycol and ethoxyethanol, respectively). The former method has an advantage in that the bimetallic nanoparticles can be prepared even at a Cu : Pd ratio higher than 1.

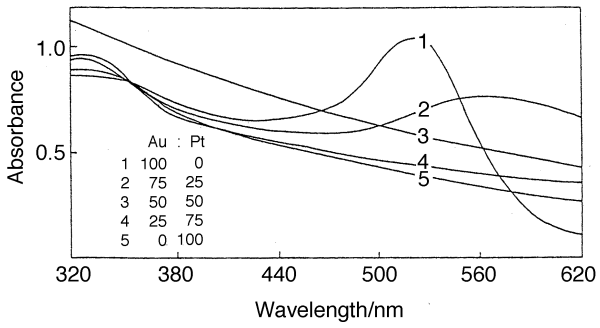

Fig. 4 UV/VIS spectra of Au–Pt bimetallic nanoparticles prepared by citrate reduction. (Reprinted with permission from ref. 80. Copyright 1981 Kodansha)

In the case of the modified alcohol reduction procedure,[86–88] metal hydroxides are prepared first by pH control of the ionic solutions. The reduction system should be kept under nitrogen to avoid re-oxidization by air. Water of crystallization in the metal salt molecules are eliminated by keeping the solution at high temperature. Therefore, only an air-cooled condenser was equipped onto the reaction flask.

Copper sulfate, palladium acetate, and PVP are dissolved in glycol, followed by adjustment of the pH value to 9.5–10.5 by dropwise addition of NaOH, to obtain the metal hydroxide. The color of the solution changed from yellow to green, which indicates formation of metal hydroxide. Refluxing the solution at 198 °C with a nitrogen flow to remove water from the system for 3 h gave a stable homogeneous dark-brown solution of the PVP-stabilized Cu–Pd bimetallic nanoparticles. Monometallic nanoparticles can also be prepared by this procedure. Cu nanoparticles have a diameter of more than 100 nm, but the diameter of Cu–Pd bimetallic nanoparticles is less than 2 nm, which suggests that the simultaneous reduction of Cu and Pd ions produces alloyed nanoparticles. Auger and XPS spectroscopies indicated that these nanoparticles contain Cu^0 species.

PVP-stabilized Ni–Pd and Ni–Pt bimetallic nanoparticles could also be prepared by a similar method.[89]

Thermal decomposition of metal acetates in the presence of PVP was proposed by Bradley *et al.*,[90] where the preparative procedure of Esumi *et al.*[91] was modified. Thus, heating of palladium and copper acetates in a solvent with high boiling point (ethoxyethanol) provides PVP-stabilized Pd–Cu bimetallic nanoparticles. In this method, not only thermal decomposition but also reduction by ethoxyethanol, as in our modified alcohol reduction method, could be involved. However, the Bradley method can provide Cu–Pd bimetallic nanoparticles that contain less than 50 mol% of Cu, while our method can provide particles with 75 mol% of Cu. In Esumi's original procedure, methyl *iso*-butyl ketone (MIBK) was used as a solvent without a stabilizer. In his method, Cu^{II} was not completely reduced to Cu^0, but Cu_2O was involved in the bimetallic nanoparticles. Probably, thanks to Cu^I species, no stabilizer is necessary for a stable dispersion.

Remita *et al.* proposed the synthesis of poly(vinyl alcohol) (PVA)-stabilized Ag–Pt bimetallic nanoparticles by radiolysis of an aqueous mixture of Ag_2SO_4 and K_2PtCl_4 at a concentration of 10^{-4} mol dm^{-3}, which showed no precipitate of AgCl.[92] Fig. 5 shows the UV/VIS spectra of ^{60}Co γ-irradiated aqueous mixtures of Ag_2SO_4 and K_2PtCl_4. A 100% Ag solution shows a typical Ag plasmon absorption band at *ca.* 410 nm. However, Ag–Pt (60 : 40) shows only a low-intensity plasmon absorption, which indicates that Ag–Pt bimetallic nanoparticles were formed by the γ irradiation. When PAA, poly(acrylic acid), was used as the stabilizer, the resulting UV/VIS spectra were quite different, as shown in Fig. 6. With PAA, however, Ag–Pt bimetallic nanoparticles were formed as well.

Henglein also proposed to use γ radiolysis to produce bimetallic nanoparticles of noble metals.[93] Silver particles having a gold layer were prepared and the UV/VIS absorption spectra of these bimetallic nanoparticles were intensively investigated. Several noble metal ions were deposited onto Ag sols to produce bimetallic nanoparticles.[93,94] Hg ions can be reduced in the presence of Ag sol, which results in the formation of Hg shell-type Hg–Ag bimetallic nanoparticles.[95,96]

Harriman reported the co-reduction of $HAuCl_4$ and H_2PtCl_6 in the presence of a non-ionic surfactant (Carbowax) by γ radiolysis.[97] However, photochemical co-reduction of $HAuCl_4$ and H_2PtCl_6 in the presence of poly(ethylene glycol) monolaurate generates only the mixture of monometallic

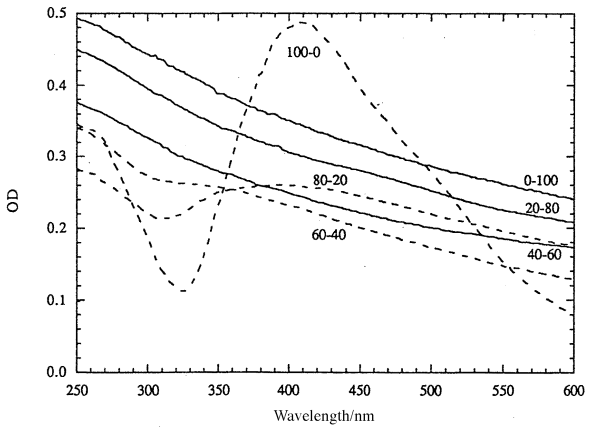

Fig. 5 UV/VIS spectra obtained for irradiated solutions containing Ag_2SO_4 and K_2PtCl_6 in various ratios in the presence of PVA. Dose for total metal reduction. (Reprinted with permission from ref. 92. Copyright 1996 Elsevier Science)

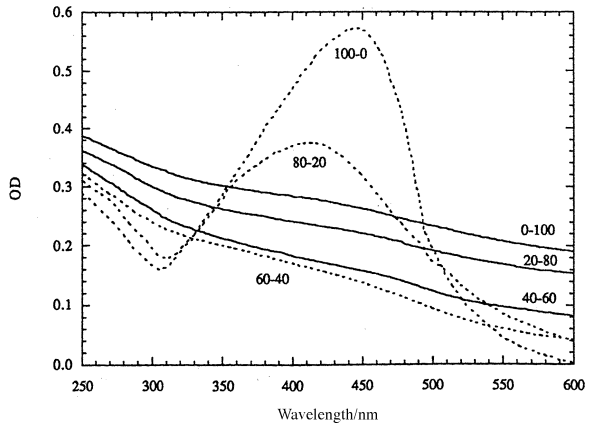

Fig. 6 UV/VIS spectra obtained for irradiated solutions containing Ag_2SO_4 and K_2PtCl_6 in various ratios in the presence of PAA. Dose for total metal reduction. (Reprinted with permission from ref. 92. Copyright 1996 Elsevier Science)

nanoparticles.[98] Probably, the non-miscibility of Au and Pt, the very weak coordination of metal ions and/or atoms to the stabilizer, and the slow rate of photo-reduction result in the formation of monometallic nanoparticles in this case.

In the co-reduction of the corresponding two metal salts by tetraoctylammonium triethylhydroborate in THF, Pt–Ru [99] and Pt–Rh[18,100] bimetallic nanoparticles stabilized by tetraoctylammonium bromide were obtained. No metal borate was found in the product.

Surfactant-stabilized light transition metal–precious metal bimetallic nanoparticles were also prepared.[101] For example, in the preparation of Pd–Sn bimetallic nanoparticles, separate boiled clear solutions of $SnCl_2$ and $Pd(NO_3)_2$ with a small portion of concentrated HCl were mixed and evaporated to dryness. The dry solids were digested with concentrated HNO_3 and HCl, forming an orange-red solution, which was again evaporated. The dry solid was then extracted with water and reduced by borohydride in the presence of surfactant. In the Pd–Sn bimetallic nanoparticles thus prepared, tin exists as Sn^{II} or Sn^{IV} ions, as confirmed by XPS.

2.2.2 Successive reduction of metal ions. Successive reduction of two metal salts can be considered as one of the most suitable methods to prepare core–shell structured bimetallic particles. In 1970, Turkevich and Kim tried to grow gold on Pd nanoparticles to obtain gold-layered Pd nanoparticles.[67] The deposition of one metal element on pre-formed monometallic nanoparticles of another metal seems to be very effective. For this purpose, however, the second element must be deposited on the surface of pre-formed particles, and the pre-formed monometallic nanoparticles must be chemically surrounded by the deposited element.

An attempt to prepare PVP-stabilized Au–Pd bimetallic nanoparticles was made by the successive reduction procedure.[102] When preparation of Au nanoparticles precedes the reduction of Pd ion, only mixtures of Pd and Au monometallic nanoparticles were produced. On the other hand, when the preparation of Pd nanoparticles precedes the reduction of Au ion, some bimetallic nanoparticles were found. However, the Au–Pd bimetallic nanoparticles thus obtained did not have a core–shell structure, although the bimetallic nanoparticles obtained by the co-reduction have such a structure. This difference in the structure may be due to the redox potentials of Pd and Au ions. When Au ions are added in the presence of Pd nanoparticles, some Pd^0 atoms on the nanoparticles are oxidized and reduce Au^{III} ions to Au^0 atoms. After the reduction of Au^{III} ions, the oxidized Pd ions are reduced again by the reductant such as an alcohol. This process may form particles with a complex ('cluster-in-cluster') structure. Pd core–Au shell nanoparticles were not produced by this process.

Ligand-stabilized Au–Pd [57] and Au–Pt [103] bimetallic nanoparticles were prepared by Schmid *et al.* by successive reduction. Au colloids, with a diameter of *ca.* 18 nm, could be covered by Pt or Pd shells when the chloride precursors, H_2PtCl_6 or $PdCl_2$, were reduced. The original red color due to the Au nanoparticles changed to brown-black when covered with Pt and Pd atoms. Addition of the water-soluble ligand *p*-($H_2NC_6H_4SO_3Na$) stabilized the obtained bimetallic nanoparticles.

In the case of Au–Pt bimetallic nanoparticles, uniform heterogeneous agglomerates with a large spherical Au core surrounded by small (≈5 nm diameter) spherical Pt particles were obtained. By EDX measurements, only Pt was found on the surface of the bimetallic agglomerates. Probably, a broad miscibility gap between 2 and 85 wt% Au causes this phenomenon.[103]

In the Au–Pd bimetallic case, on the contrary, a rather continuous structure was formed. TEM investigations of Au–Pd bimetallic nanoparticles show somewhat irregular structures,

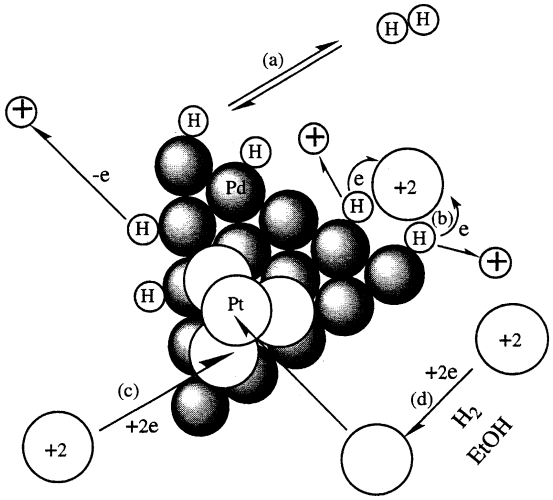

Fig. 7 Sacrificial hydrogen protective strategy for the preparation of bimetallic nanoparticles with a Pd shell–Pt core structure. (Reprinted with permission from ref. 106. Copyright 1997 American Chemical Society)

but no agglomeration of small particles was observed. The EDX spectrum of such a single particle showed only Pd on the surface. The reverse successive reduction also worked and Pd core–Au shell structured bimetallic nanoparticles were produced.

In an earlier study, Turkevich and Kim proposed gold-layered palladium nanoparticles.[67] Three types of Au–Pd bimetallic nanoparticles, such as Au core–Pd shell, Pd core–Au shell and random alloyed particles were prepared by the application of successive reduction.[104] Two kinds of layered Pd–Pt bimetallic nanoparticles were also reported by successive reduction.[105] However, detailed analyses of the structure of these bimetallic nanoparticles were not carried out at that time. Only the difference of UV/VIS spectra between the bimetallic nanoparticles and the physical mixtures of the corresponding monometallic nanoparticles were discussed.

Let us compare the results of Schmid and coworkers with ours. In our case, PVP-stabilized Au–Pd bimetallic nanoparticles, prepared by successive reduction, could not generate a core–shell type of bimetallic nanoparticles. Compared to this, in Schmid's case the size of the Pd core is much larger than in our case. During the reduction of $AuCl_4^-$, the oxidation of Pd^0 atoms may also occur in the system of Schmid and coworkers. However, because of their large size, before the decomposition of Pd core particles, generated Au atoms may precipitate on them, thus also protecting Pd from further oxidation.

Recently, our group has invented the modified successive alcohol reduction process to prepare 'reversed core–shell' structured bimetallic nanoparticles.[106] In practice, PVP-stabilized Pd core–Pt shell bimetallic nanoparticles with a size of *ca.* 2 nm were obtained. Precious metals like Pd have the ability to adsorb hydrogen and split it to form metal—H bonds on the surface. Hydrogen atoms adsorbed on precious metal atoms have a very strong reducing ability, implying a quite low redox potential. As illustrated in Fig. 7, Pt ions added into the dispersion of Pd nanoparticles are reduced by hydrogen atoms adsorbed on the pre-formed Pd nanoparticles without oxidizing Pd atoms to Pd ions, and are deposited on the Pd nanoparticles to form Pd core–Pt shell bimetallic nanoparticles.

2.2.3 Reduction of double complexes. Except for Ag–Au bimetallic nanoparticles, bimetallic nanoparticle dispersions containing Ag have not been studied extensively. As possible reasons for this, it should be noted that Ag^I ion readily reacts with halide ions to produce water-insoluble silver halides. Also, many other water-soluble metal salts other than halides are not so suitable as precursors for the production of metallic particles by mild reduction.

Torigoe and Esumi proposed silver(I) bis(oxalato)palladate(II) as a precursor of Ag–Pd bimetallic nanoparticles stabilized by PVP.[107] Photo-reduction of the aqueous precursor in a quartz vessel gave Ag–Pd bimetallic nanoparticles at various concentrations. The particles deviate from spherical ones but are uniform, and each particle contains both metal elements, as confirmed by EDX measurement. The size changed with concentration of the precursor. The average composition of bimetallic nanoparticles became Ag-rich with increasing concentration of the precursor, which could be confirmed by EDX and UV/VIS spectral investigations.

Preparation of PVP-stabilized Ag–Pt bimetallic nanoparticles by borohydride reduction from silver(I) bis(oxalato)platinate(I) was also proposed.[108]

2.2.4 Electrochemical formation of bimetallic nanoparticles. Most chemical methods for the preparation of metal nanoparticles are based on the reduction of the corresponding metal ions with chemical reagents and on the controlled aggregation of the obtained metal atoms. Instead of chemical reduction, an electrochemical process can be used to create metal atoms from bulk metal. Reetz and Helbig proposed an electrochemical method including both oxidation of bulk metal and reduction of the metal ions for size-selective preparation of tetraalkylammonium salt-stabilized metal nanoparticles (Fig. 8).[109] The particle size could be controlled by the current density.

The Pd–Pt, Ni–Pd, Fe–Co and Fe–Ni bimetallic nanoparticles could be also obtained by this method.[110,111] Bulk plates of two metal elements were immersed as anodes into electrolyte containing a stabilizer (tetraalkylammonium salt) and a Pt plate was used as a cathode. From the anodes the corresponding metal ions were generated, and the generated metal ions were reduced by electrons generated from the Pt cathode to produce tetraalkylammonium salt-stabilized bimetallic nanoparticles. The advantages of this method include low cost, high yield, easy isolation and simple control of the metal content of the bimetallic nanoparticles.

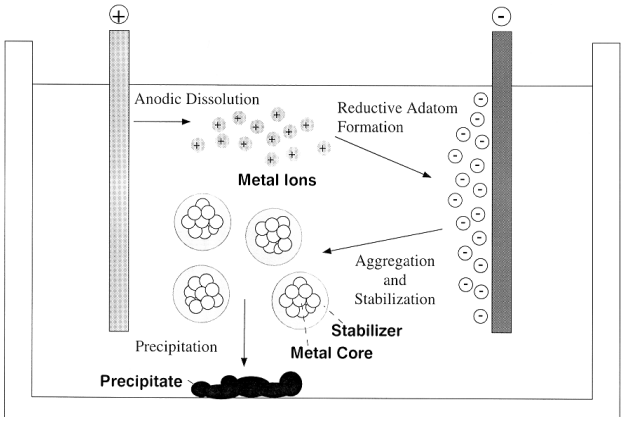

Fig. 8 Formation scheme of electrochemically produced metal nanoparticles. (Adapted from ref. 109. Copyright 1994 American Chemical Society)

3 How to Characterize Bimetallic Nanoparticles

In this section, we would like to briefly introduce some characterization methods of bimetallic nanoparticles. A detailed review on nanoparticle characterization was recently published, which should be consulted for further information.[112]

3.1 TEM observations

The first question asked about metal nanoparticles is concerned with aggregation state, size and morphology. Many techniques have been used to reveal the size and homogeneity of metal nanoparticles obtained by chemical methods. As distinct from small organometallic molecules, the composition of metal nanoparticles cannot be so exactly controlled as to be written down as $M_n M'_{n'}$. However, the homogeneity of particle size or shape on the atomic scale is quite important to reveal the physical properties of nanosized materials.

Amongst the techniques commonly used, transmission electron microscopy (TEM) is indispensable for metal nanoparticle studies. Metal nanoparticles, especially those consisting of heavy (precious) metal elements, give high contrast when the particles are dispersed on thin carbon films supported by metal grids.

Sample preparation of colloidal dispersions of metal nanoparticles for TEM observation is quite simple, involving evaporation of a small drop of dispersion onto a carbon-coated microgrid. However, the carbon coating must be thin enough to obtain a good contrast. Further, if the dispersion contains many additives, such as stabilizers or ligands, it may be diluted or filtered to obtain a clear view.

Thanks to a recent improvement to a high-voltage electron beam technique, the resolution of transmission electron microscopy is now sufficient to have a clear image of metal nanoparticles at the Angstrom level. Further, high resolution TEM (HRTEM) can now provide information not only on the particle size and shape but also on the crystallography of monometallic and bimetallic nanoparticles.

For large crystalline metal nanoparticles, HRTEM can suggest the area composition by the fringe measurement, giving crystal information of nanoparticles observed in the particle images.[17,113,114] Furthermore, in the case of supported metal particles, particle growth can be directly seen by *in-situ* TEM observation.

When energy disperse X-ray microanalysis (EDX) is used in conjunction with TEM, localized elemental information can be obtained.[103,115]

3.2 UV/VIS spectroscopy

The property most immediately observable for metal nanoparticle dispersions of certain metals is their color. Faraday's classical Au sol shows even now the clear ruby-red color. Ruby glasses, with included Au nanoparticles, are very famous. Indeed, Au, Ag and Cu (Group 1B metal) nanoparticles all have characteristic colors related with their particle size. Thus, for these metals, observation of UV/VIS spectra can be a useful complement to other methods in characterizing metal particles.

Comparison of spectra of bimetallic nanoparticles with the spectra of physical mixtures of the respective monometallic particle dispersions can confirm a bimetallic structure for the nanoparticles.[80,116] Furthermore, with the goal of revealing the formation processes of bimetallic nanoparticles, that is, the reduction of metal ions and the aggregation process, the observation of UV/VIS spectral changes during reduction can provide quite important information, which will be discussed in detail later.[117]

3.3 IR spectroscopy

Infrared spectroscopy has been widely applied to the investigation of the surface chemistry of adsorbed small molecules. Carbon monoxide, which can be easily adsorbed on metals, is frequently studied. Adsorbed CO is found not only in on-top sites but also in twofold or threefold sites, depending on the variation of metal and surface structure. The wavenumber of adsorbed CO changes dramatically with the binding structure.[19,24,34,118] IR spectroscopy of CO on the surface of bimetallic nanoparticles can also give some information about the surface structure of bimetallic nanoparticles. By comparison of IR spectra of CO on a series of bimetallic nanoparticles at various metal compositions, one can elucidate the surface micro-structure of bimetallic nanoparticles.[106,118]

3.4 X-Ray methods

X-Ray methods are informative for nondestructive elemental and structural analyses. X-Ray diffraction gives structural information on nanoparticles, including qualitative elemental information. Characteristic X-ray absorption, electron emission by X-ray bombardment and X-ray emission by electron irradiation give clear information on the varieties and amounts of the elements contained in nanoparticles. Here, we would like to summarize some X-ray methods often used for the characterization of bimetallic nanoparticles.

3.4.1 X-Ray diffraction (XRD). X-Ray diffraction is a strong method to investigate the solid structure of metal nanoparticles. For monometallic nanoparticles, the phase changes with increasing diameter of nanoparticles can be investigated with XRD. The presence of bimetallic particles as opposed to a mixture of monometallic particles can also be demonstrated by XRD since the diffraction pattern of the physical mixtures consists of overlapping lines of the two individual monometallic nanoparticles and is clearly different from that of the bimetallic nanoparticles. However, when these metals are divided into small nanoparticles consisting of less than hundreds of atoms, the acquisition of structural information may be difficult. Sometimes particles have an amorphous form and the interatomic lengths may change in small particles. In such cases, comparison of the diffractograms of bimetallic nanoparticles with those of the corresponding monometallic nanoparticles and their physical mixtures is necessary to obtain correct information. The structural model of bimetallic nanoparticles can be proposed by comparing the observed XRD spectra and computer-simulated ones.[119]

3.4.2 X-Ray photospectroscopy (XPS). With the physical analysis methods, such as TEM observation and XRD measurement, it is now well-understood that the PVP-stabilized bimetallic nanoparticles have an 'alloyed' structure. For a rationalization of their catalytic properties, the surface composition and structure are indispensable information and quantitative XPS analysis is a powerful tool in the elucidation of the surface composition.

In the case of polymer- or surfactant-stabilized metal nanoparticles, XPS cannot work well if the XPS samples are prepared by evacuation of the dispersion of nanoparticles, because the stabilizer makes a thick organic coating on the nanoparticle surface. Wang and Liu reported recently the so-called 'coordination capture' method, in which nanoparticles can be adsorbed on thiol-modified silica supports leaving free polymers and/or surfactants in solution (Fig. 9).[120] This process can also be considered as one of the pioneer studies of two-dimensional immobilization of metal nanoparticles onto a solid substrate, one of the hot topics in nanosize materials.[121–124] A potential problem of the coordination

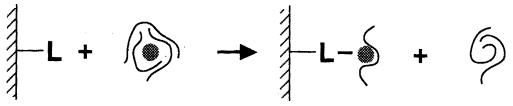

Fig. 9 Immobilization process of polymer-stabilized metal nanoparticles by the coordination capture method. (Adapted from ref. 120. Copyright 1991 Springer-Verlag)

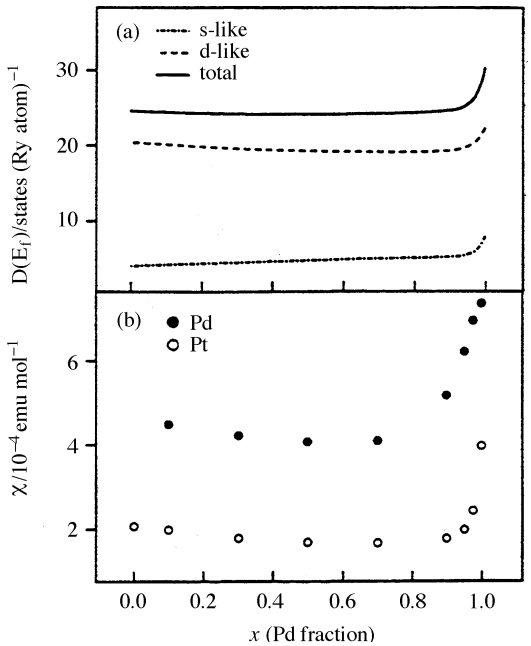

Fig. 10 (*a*) Variation of the s-like, d-like and total densities of state on 'average' Pt sites in bulk $Pt_{1-x}Pd_x$ with x, as deduced from NMR data. (*b*) Variation of the local susceptibility on Pt and Pd sites, as deduced from the curves in (*a*) and from experimental data on alloy susceptibilities. (Reprinted with permission from ref. 43. Copyright 1996 American Chemical Society)

capture method is the possibility of structural change during the process because of the change in ligand coordination.

By the quantitative analysis of XPS spectra of bimetallic nanoparticles, we can see which elements are present in the surface region of the nanoparticles.

3.4.3 Extended X-ray absorption fine structure (EXAFS). EXAFS is one of the most powerful characterization methods for obtaining the detailed structure of finite-sized materials, and in particular of metal nanoparticles. Thanks to big synchrotron radiation facilities, such as KEK in Tsukuba (Japan) and ESRF in Grenoble (France), EXAFS has become a widely used tool for scientists in many fields to determine the structure of complex materials. The specific X-ray absorption spectrum of each metal element contains various information such as identity, electron density, the number of metal elements surrounding the X-ray absorbing metal, and their interatomic distances involved in the various coordination shells. With EXAFS data from small multimetallic nanoparticles, one can calculate the number of surrounding atoms of each adsorbing metal element and estimate a possible structure of the particles in the sample.

Sinfelt *et al.* carried out major studies on the EXAFS of supported bimetallic nanoparticles, for example, Ir–Rh,[78] Cu–Ru [77] and Cu–Os.[79] This work has been well-reviewed by Sinfelt himself.[60]

Colloidal dispersions of metal nanoparticles have been successfully analyzed by EXAFS.[81,84,100,118,125–127] For example, Bradley *et al.* prepared Cu–Pd bimetallic nanoparticles by deposition of zerovalent Cu atoms onto pre-formed Pd nanoparticles.[118] Cu atoms were zerovalent on Pd nanoparticles but subsequently they migrated into the Pd particle and only a few atomic layers were found on the surface. Kolb *et al.* used the EXAFS method to study surfactant-stabilized Pd–Pt bimetallic nanoparticles, whose structure was elucidated as a Pt enriched core–Pd enriched shell-type structure.[126] EXAFS data with high precision can be obtained if the concentration of the X-ray adsorbing metal is quite high. However, higher loading of metals on inorganic supports often results in larger particles. In contrast, colloidal dispersions of nanoparticles can be made at a low concentration of metal and the particles in the dispersions can be small and uniform. EXAFS samples can be obtained by concentrating the dispersions without aggregation, to give data of high quality.

3.4.4 Energy disperse X-ray microanalysis (EDX, EDAX, EDS). One of the most revealing analytical methods for the composition of bimetallic nanoparticles is energy dispersive X-ray spectroscopy (EDX), which is usually coupled with a transmission electron microscope with high resolution.[103,107,128,129] EDX is a kind of EPMA (electron probe microanalysis) or XMA (X-ray microanalysis) method, which has higher sensitivity than the usual EPMA or XMA techniques, thanks to the lack of a prism. The electron beam can be focused on a single particle by TEM, to get information from *individual* particles. Each element in the chosen nanoparticle emits X-rays at characteristic energies by electron beam irradiation, and their intensity is proportional to the concentration of each element in the particle. This method provides analytical data that cannot be obtained by the other three methods mentioned above. For sufficiently large particles, the electron beam can be spotted on the surface area or on the center of the particle, to investigate the regional composition, which often reveals non-uniformity in the composition. Such variations of *each* particle are important when we consider the structure or the preparative process of these bimetallic nanoparticles.

3.5 Metal NMR spectroscopy

NMR spectroscopy of metal isotopes[41,130,131] is a powerful technique for understanding the electronic environment of metal atoms in metallic particles by virtue of the NMR shifts caused by free electrons (so called Knight shifts).[132]

The NMR spectra of metal nanoparticles, having Pauli paramagnetic properties, are governed both by the density of energy levels at the Fermi energy and by the corresponding wave function intensities of each site: the local density of states (LDOS). From NMR spectra of ^{195}Pt, the variations of s-like and d-like LDOS in Pt nanoparticles can be deduced (Fig. 10). This depends on the coordination of metal atoms, which can indicate bimetallic formation. Further, the electronic properties of metal nanoparticles may be informative for investigating catalytic properties of the metal nanoparticles.

^{13}C NMR and ^{1}H NMR are also quite useful to understand the structure of adsorbed organic molecules onto the surface of metal nanoparticles.[19,20,133–135] (Refer to the detailed review published earlier.[112])

4 Structure of Bimetallic Nanoparticles

In bulk metals, atoms are arranged in various geometries, each metal having its own mode of atom placement. The resulting crystal structure is usually simple and depends on the identity of the metal and other conditions such as temperature. In the case of nanoparticles of metals, the three-dimensional arrangement of atoms may be similar to the crystal structure of the corresponding bulk metal, but in some cases they may have a rather amorphous structure, depending on preparative conditions.

Bimetallic nanoparticles, which are composed of two kinds of metal elements, can have the crystal structure similar to the bulk alloy as well. In addition, they can adopt another type of structure, in which the distribution of each metal element is not that found in the bulk. Such structures, defined by the distribution modes of the two elements, include the random

alloy, alloy with an intermetallic compound type, cluster-in-cluster, and core–shell structure.

In this section, we would like to introduce these bimetallic structures in detail based on the results of structural analyses of practical bimetallic nanoparticles. In fact, detailed structural information is quite essential to understand the properties of bimetallic nanoparticles. One analytical method, even a powerful one such as EXAFS, is not enough to elucidate the detailed structure of bimetallic nanoparticles. Several analysis methods must be combined.

4.1 Core–shell structure

In a core–shell structure, one metal element forms an inner core and the other element surrounds the core to form a shell. This bimetallic structure is characteristic of PVP-stabilized bimetallic nanoparticles of precious metals. A typical example has been observed in PVP-stabilized Pd–Pt bimetallic nanoparticles.

4.1.1 PVP-stabilized Pd–Pt bimetallic nanoparticles. PVP-stabilized Pd–Pt bimetallic nanoparticles were prepared by alcohol reduction from a mixture of H_2PtCl_6 and $PdCl_2$. These bimetallic nanoparticles were analyzed in detail by several methods.[81,82,116] Here, we would like to demonstrate the detailed analytical procedures using Pd–Pt bimetallic nanoparticles as an example.

First, TEM observation was carried out on these bimetallic nanoparticles. In Fig. 11, the average diameter and size distributions of PVP-stabilized Pd–Pt bimetallic nanoparticles with various metal compositions are displayed. One can see clearly in this figure that the particle size depends on the metal composition and the minimum was obtained at Pd : Pt = 4 : 1 (mol/mol). In particular, Pd–Pt bimetallic nanoparticles at a Pd : Pt mole ratio of 4 : 1 show excellent uniformity in size and the average diameter is 1.5 nm. This average diameter indicates that the Pd–Pt (4 : 1) bimetallic nanoparticles consist of 55 atoms in a particle on average, if we choose the nearest magic (closed-shell) number,[136] analogous to the Au_{55} nanoparticle prepared by diborane reduction of an Au^I precursor, which is a mild reduction procedure, proposed by Schmid *et al.*[14] This indicates that the bimetallic nanoparticle, not the physical mixture, was formed by co-reduction of the two metal salts.

The contrast in TEM images of metal nanoparticles observed also gives important information. Pt monometallic nanoparticles show a clear contrast, while Pd monometallic nanoparticles show a light gray image. Clear contrast was not observed for Pd–Pt bimetallic nanoparticles with an average diameter of 1.5–3 nm, from which one can estimate that both elements will be contained by each particle and that Pd may be concentrated on the surface of these bimetallic nanoparticles.

UV/VIS spectra of these dispersions are collected in Fig. 12. The absorption peaks that are found in the spectra of Pt and Pd ionic precursors completely disappear after refluxing the alcohol solution of mixed metal ions in the presence of PVP, showing the completion of reduction of both ions. Pd–Pt bimetallic nanoparticle dispersions show similar spectra as that of Pd monometallic dispersion in the region of 500–850 nm, but at shorter wavelengths (250–450 nm) the absorbance of Pd–Pt bimetallic nanoparticles is larger than Pd. In this wavelength region, the larger the Pt ratio the larger is the absorbance of the bimetallic nanoparticle dispersions. The spectra of bimetallic nanoparticle dispersions were found not only to differ from those of monometallic dispersions, but also from those of physical mixtures. These results do not directly suggest the core–shell structure, but can suggest the formation of bimetallic nanoparticles.

XRD spectra of the monometallic Pd and Pt nanoparticles, the Pd–Pt (1 : 1) bimetallic nanoparticles and the physical mixture (1 : 1) of Pd and Pt monometallic nanoparticles are collected with those of other nanoparticles in Figs. 13 and 14. Pd monometallic nanoparticles do not have diffraction peaks as narrow as those of Pt and Au nanoparticles. Bradley *et al.* showed, on the basis of electron scattering, that Pd nanoparticles with a diameter less than 2.0 nm can be poorly crystalline or possibly amorphous,[24] on the basis of weak, broad electron diffraction rings. The average diameter of Pd nanoparticles whose XRD spectrum is shown here is *ca.* 2.5 nm. These three elements show an fcc structure in the bulk and from these XRD patterns these nanoparticles can be considered to have also an fcc structure. In the case of Pd–Pt bimetallic nanoparticles, some differences can be found between the two XRD patterns of the physical mixtures and the bimetallic nanoparticles. The spectrum of the bimetallic nanoparticles has wider peaks than that of the mixtures, showing that the nanoparticles have less ordered structures, which may suggest the formation of bimetallic bonds, that is, three kinds of metal bonds (Pd–Pd, Pd–Pt and Pt–Pt) in each particle.

XPS analyses of PVP-stabilized Pd–Pt bimetallic nanoparticles at 1 : 1 mole ratio were carried out by using the coordination capture method (see above).[120] The result is shown in Table 2, and clearly indicates that Pd atoms are preferentially located on the surface region rather than the inside. The XPS method is simple but informative enough for understanding the catalytic properties of bimetallic nanoparticles, which are dominated mainly by the metal composition and structure of the nanoparticle surface.

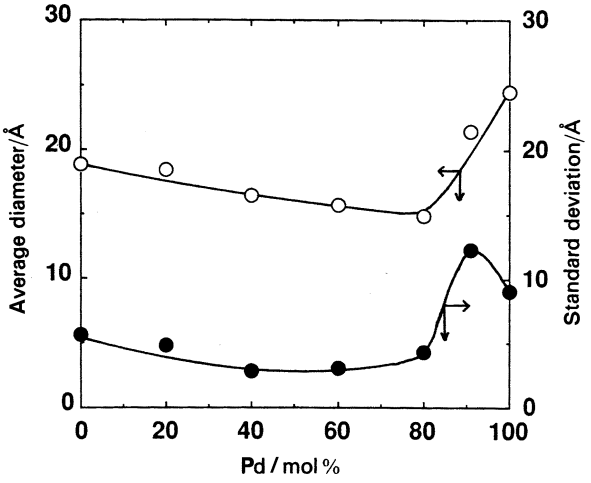

Fig. 11 (○) Average diameter and (●) standard deviation of PVP-stabilized Pd–Pt bimetallic nanoparticles as a function of the Pd content. (Reprinted with permission from ref. 83. Copyright 1993 Royal Society of Chemistry)

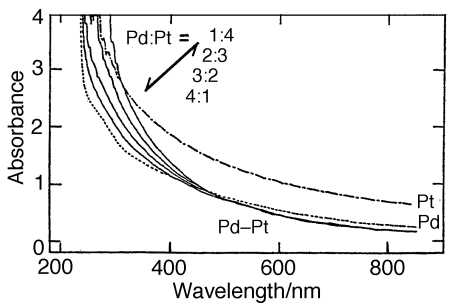

Fig. 12 UV/VIS absorption spectra of PVP-stabilized Pd and Pt monometallic nanoparticles and Pd–Pt bimetallic nanoparticles. (Reprinted with permission from ref. 81. Copyright 1991 American Chemical Society)

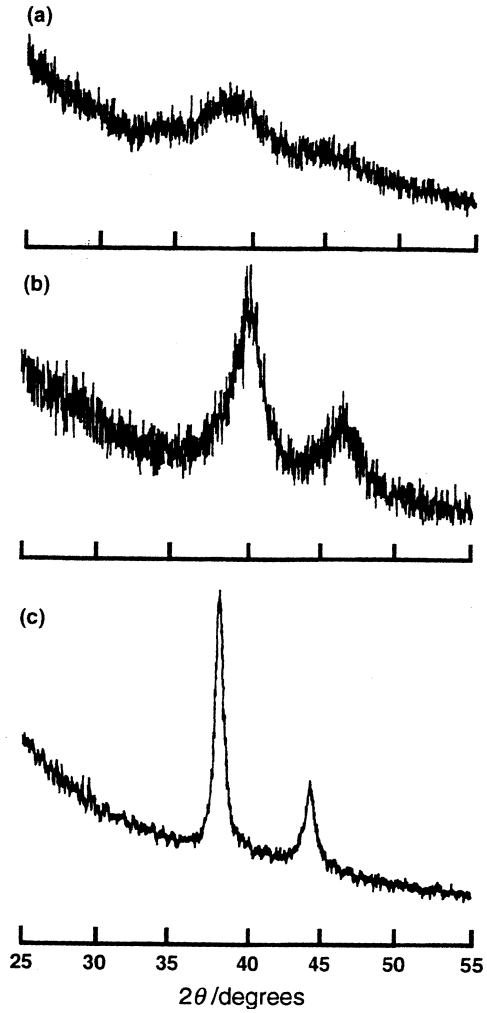

Fig. 13 X-Ray diffractograms of PVP-stabilized (*a*) Pd, (*b*) Pt and (*c*) Au monometallic nanoparticles. (Reprinted with permission from ref. 117. Copyright 1995 Royal Society of Chemistry)

To obtain more detailed information about the structure of Pd–Pt bimetallic nanoparticles, an EXAFS investigation was carried out. This was the first example of the structural definition of bimetallic nanoparticles by EXAFS with monometallic and alloy foils as references. Until now, many reports on EXAFS analyses of bimetallic nanoparticles have appeared,[84,100,118,126] but proposals of a complete model for bimetallic nanoparticles were only achieved by us with these detailed analyses.

Table 2 Quantitative XPS data of polymer-protected bimetallic clusters[a]

Sample	Observed band	Relative intensity
Pd–Pt	Pd_{3d} $Pt_{4d\ 5/2}$	Pd/Pt = 2.06
Au–Pd	Pd_{3d} Au_{4f}	Pd/Au = 1.84
Au–Pt	$Pt_{4d\ 5/2}$ Au_{4f}	Pt/Au = 1.57

[a] Reprinted with permission from ref. 117. Copyright 1995, Royal Society of Chemistry.

Sample preparation for EXAFS analyses of colloidal dispersion of metal nanoparticles is simple.[81] To obtain EXAFS data with a good accuracy, which of course depends on the strength of the beam, higher loading of target precious metal elements is desirable. Therefore, the dispersions of metal nanoparticles should be concentrated or metal nanoparticles should be collected in a powder form.

In order to understand, first of all, the detailed structure of PVP-stabilized Pd–Pt bimetallic nanoparticles prepared by *simultaneous* alcohol reduction, we analyzed Pd foil, Pt foil, Pd–Pt (1 : 9) foil, Pd–Pt (1 : 1) foil and Pd–Pt (9 : 1) foil to obtain bulk data and the parameter of the heterogeneous metal–metal bond (M—M′).[81] Then, Pd and Pt monometallic nanoparticles were examined. With these parameters, Pd–Pt bimetallic nanoparticles were analyzed.

Fig. 15 shows the Fourier transforms of Pd K edge EXAFS of the Pd monometallic and the Pd–Pt bimetallic nanoparticle dispersions. The main strong peak found in the spectrum of Pd monometallic nanoparticles can be assigned to the Pd—Pd metal bond, which was confirmed and determined to be 0.274 nm by the curve-fitting analysis. In the spectrum of Pd–Pt (4 : 1) bimetallic nanoparticles, the main peak mentioned above has a shoulder, attributed to the Pd—Pt bond as well as to the Pd—Pd bond, because the phase shift arises from the interference between the Pd atom and the Pt atoms surrounding Pd. The coordination numbers and interatomic distances were determined by the curve-fitting method. In Table 3 the obtained data from Pd K edge and Pt L_3 edge EXAFS spectra of Pd–Pt (4 : 1) bimetallic nanoparticles are

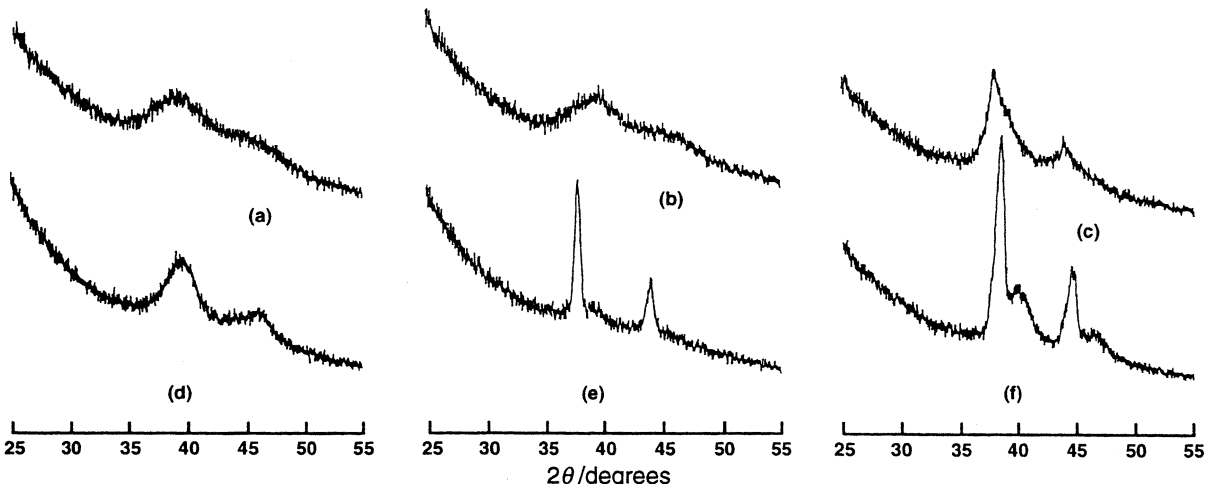

Fig. 14 X-Ray diffractograms of PVP-stabilized (*a*) Pd–Pt (1 : 1), (*b*) Au–Pd (1 : 1) and (*c*) Au–Pt (1 : 1) bimetallic nanoparticles and of 1:1 physical mixtures of PVP-stabilized monometallic (*d*) Pd + Pt, (*e*) Au + Pd and (*f*) Au + Pt nanoparticles. (Reprinted with permission from ref. 117. Copyright 1995 Royal Society of Chemistry)

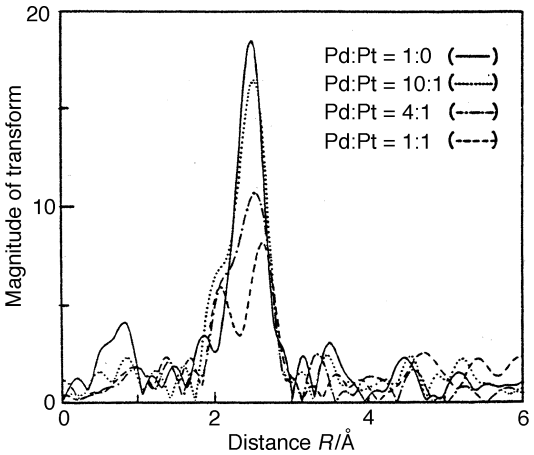

Fig. 15 Fourier-transformed EXAFS spectra (Pd K edge) of colloidal dispersions of PVP-stabilized Pd–Pt bimetallic nanoparticles at Pd : Pt ratios of 1 : 0, 10 : 1, 4 : 1 and 1 : 1. (Reprinted with permission from ref. 81. Copyright 1991 American Chemical Society)

collected. These results clearly indicate that these bimetallic nanoparticles have both metal elements in a particle.

The coordination numbers of Pd and Pt in these bimetallic nanoparticles suggest a structural model for them. From TEM observation, Pd–Pt (4 : 1) bimetallic nanoparticles have an average diameter of 1.5 nm with high uniformity, indicating that each nanoparticle contains 55 metal atoms if the magic number concept is adopted. This particle has 42 (76.4%) atoms on the surface and 13 (23.6%) atoms in the core area, which is close to the ratio 4 : 1. Assuming that all the atoms on the surface are Pd and that the core is totally filled by Pt, that is, the Pt core–Pd shell structure [Fig. 16(*a*)], the coordination numbers of both elements can be calculated as shown in Table 3.

The structure of PVP-stabilized Pd–Pt (1 : 1) bimetallic nanoparticles is also considered with EXAFS methods. Three possible models proposed are illustrated in Fig. 17(*a–c*). From

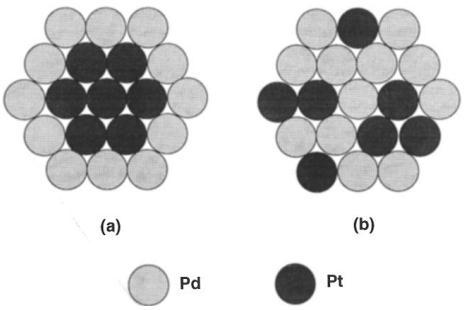

Fig. 16 Cross-sections of PVP-stabilized Pd–Pt (4 : 1) bimetallic nanoparticle models: (*a*) Pt core–Pd shell model, (*b*) random model. (Reprinted with permission from ref. 81. Copyright 1991 American Chemical Society)

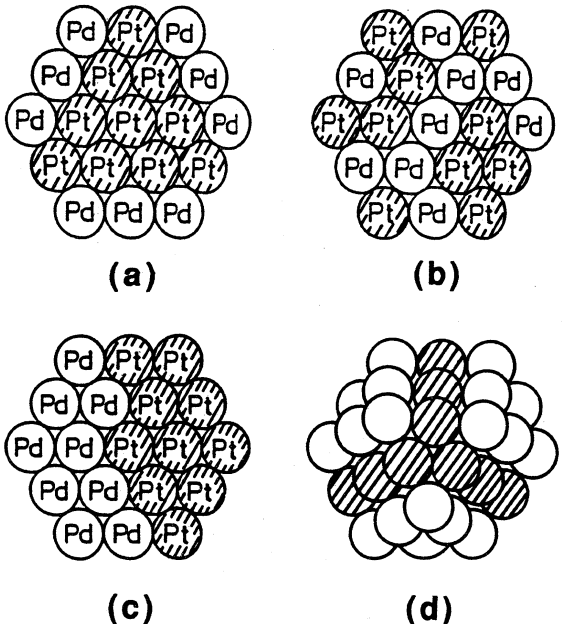

Fig. 17 Cross-sections of PVP-stabilized Pd–Pt (1 : 1) bimetallic nanoparticle models: (*a*) Pt core–Pd shell model, (*b*) random model, (*c*) separated model. (*d*) Three-dimensional picture of the Pt core–Pd shell model. (Reprinted with permission from ref. 81. Copyright 1991 American Chemical Society)

the XPS results of Pd–Pt (1 : 1) bimetallic nanoparticles shown in Table 2, one can select the modified Pt core–Pd shell model [Fig. 17(*a*)] as the best candidate.

In Table 4, the coordination numbers of both elements observed and calculated from the model proposed in Fig. 17(*a*) are collected. Comparing the EXAFS data of Pd–Pt bimetallic nanoparticles, the coordination number of Pt around Pd is larger and that of Pd around Pd is smaller in the case of Pd–Pt (1 : 1) bimetallic nanoparticles than those in the case of Pd–Pt (4 : 1) bimetallic ones. This comparison indicates that some Pt atoms are located on the surface and the fraction of Pd—Pt bonds predominates considerably in Pd–Pt (1 : 1) bimetallic nanoparticles. From these observations, the best fit model is the Pt core–Pd shell model [Fig. 17(*a*)], which can be selected from the XPS data as well. This is the first time that the detailed structure of bimetallic nanoparticles could be determined by the combination of several analytical methods: UV/VIS spectra, TEM observation, XRD spectra, XPS data and EXAFS analyses.

EXAFS analysis, which can provide the coordination number of the elements around a target element, can be also used to analyze the structural change of nanoparticles adsorbing small molecules such as oxygen.[129] In Table 5, the coordination numbers obtained by EXAFS measurement were collected in several oxidized states. The coordination numbers change gradually depending on the extent of oxidation, especially that of Pd around Pd decreases and that of oxygen

Table 3 Coordination numbers around the Pd and Pt atoms in a Pd–Pt (4 : 1) bimetallic cluster determined from EXAFS data[a]

Absorbing metal	Scattering metal	Interatomic distance r/Å	Coordination number N		
			Obsd	Pt core[b]	Random[b]
Pd	Pd	2.74 ± 0.03	4.4 ± 1.0	4.6	6.0
Pd	Pt	2.73 ± 0.03	2.3 ± 1.3	2.0	1.9
Pt	Pt	2.73 ± 0.03	5.5 ± 1.7	5.5	1.9
Pt	Pd	2.72 ± 0.03	3.5 ± 1.5	6.5	6.0

[a] Reprinted with permission from ref. 81. Copyright 1991 American Chemical Society. [b] See Fig. 16.

Table 4 Coordination numbers around the Pd and Pt atoms in a Pd–Pt (1 : 1) bimetallic cluster determined from EXAFS data[a]

Absorbing metal	Scattering metal	Interatomic distance r/Å	Coordination number N			
			Obsd	Pt core[b]	Random[b]	Separated[b]
Pd	Pd	2.74 ± 0.03	2.3 ± 1.0	3.1	3.9	6.0
Pd	Pt	2.74 ± 0.03	3.0 ± 1.1	3.0	3.9	1.7
Pt	Pt	2.73 ± 0.03	4.8 ± 1.7	6.6	3.9	6.4
Pt	Pd	2.73 ± 0.03	1.3 ± 1.0	2.9	3.9	1.6

[a] Reprinted with permission from ref. 81. Copyright 1991 American Chemical Society. [b] See Fig. 17.

around Pd increases. These changes can indicate a model for the structural change of Pd–Pt (4 : 1) bimetallic nanoparticles by oxidation as shown in Fig. 18. In the same way, Fig. 19 shows a possible model for the structural change of PVP-stabilized Pd–Pt (1 : 1) bimetallic nanoparticles by oxidation.

As described in the preparation section, Pd–Pt bimetallic nanoparticles with reverse core–shell structure, that is, a Pd core–Pt shell structure, have recently been prepared by the successive reduction procedure using a sacrificial hydrogen strategy.[106] This reverse core–shell model was proposed on the basis of the IR spectroscopic data of surface-adsorbed CO as a probe. IR spectra of CO adsorbed on the PVP-stabilized

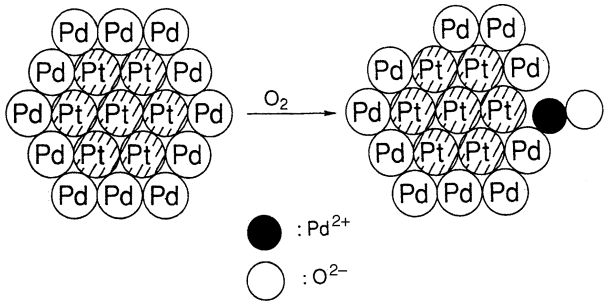

Fig. 18 Cross-section of a model for the structural changes in PVP-stabilized Pd–Pt (4 : 1) bimetallic nanoparticles induced by oxidation. (Reprinted with permission from ref. 129. Copyright 1992 American Chemical Society)

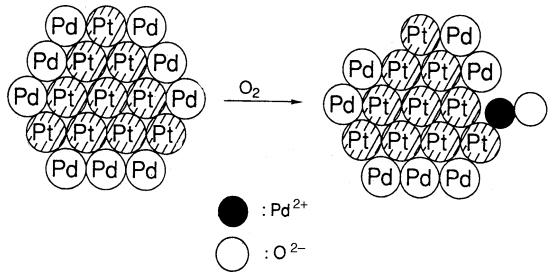

Fig. 19 Cross-section of a model for the structural changes in PVP-stabilized Pd–Pt (1 : 1) bimetallic nanoparticles induced by oxidation. (Reprinted with permission from ref. 129. Copyright 1992 American Chemical Society)

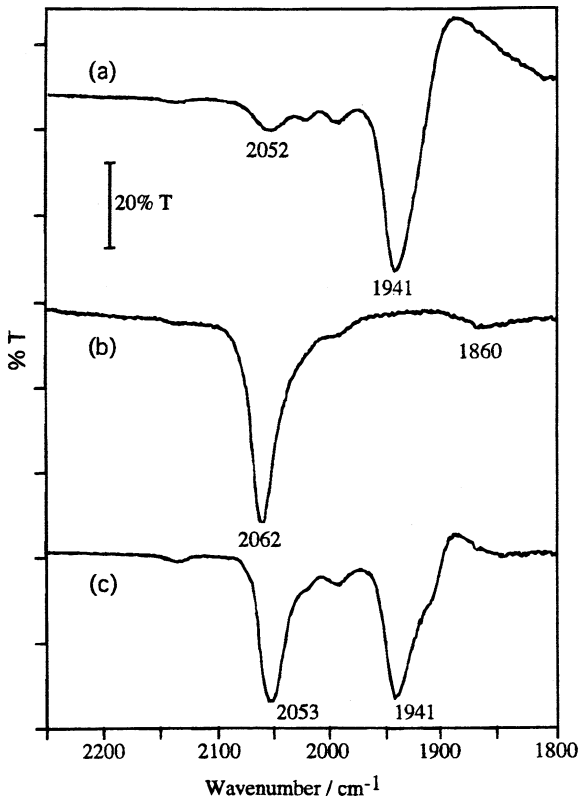

Fig. 20 FTIR spectra of CO adsorbed on PVP-stabilized Pd and Pt monometallic nanoparticles: (*a*) Pd (1.0×10^{-4} mol of Pd in 10 cm^3 of CH_2Cl_2), (*b*) Pt (1.0×10^{-4} mol of Pt in 10 cm^3 of CH_2Cl_2), (*c*) physical mixture of dispersions (*a*) and (*b*) with [Pd] = [Pt] = 5.0×10^{-5} mol in 10 cm^3 of CH_2Cl_2. (Reprinted with permission from ref. 106. Copyright 1997 American Chemical Society)

Table 5 Change in the coordination numbers of PVP-stabilized Pd–Pt (4 : 1) bimetallic nanoparticles induced by oxidation[a]

Absorbing metal	Scattering metal	Coordination number N			
		Nitrogen[b]	Air[c]	Air (3d)[d]	Air (10d)[e]
Pd	Pd	3.8 ± 0.7	3.1 ± 0.5	2.7 ± 0.4	2.3 ± 0.4
Pd	Pt	0.9 ± 0.2	0.9 ± 0.2	1.0 ± 0.2	0.5 ± 0.1
Pd	O		0.21 ± 0.02	0.36 ± 0.04	2.3 ± 0.3
Pt	Pt	5.7 ± 1.2	4.6 ± 0.8	3.9 ± 0.5	3.9 ± 0.7
Pt	Pd	3.8 ± 0.4	3.9 ± 0.3	4.2 ± 0.3	2.1 ± 0.2

[a] Reprinted with permission from ref. 129. Copyright 1992 American Chemical Society. [b] Prepared under nitrogen. [c] Prepared under air. [d] Kept for 3 days under air after having been prepared under nitrogen. [e] Kept for 10 days under air after having been prepared under air.

Pt and Pd monometallic nanoparticles, used in this successive reduction process as the core seed, are collected in Fig. 20. In the case of CO adsorbed on Pd nanoparticles, a strong band at 1941 cm^{-1}, assignable to CO adsorbed on the surface at a bridging site, and a weak band at 2052 cm^{-1} are found. In contrast, CO adsorbed on Pt nanoparticles shows a strong band at 2062 cm^{-1}, assignable to CO adsorbed on the surface at a terminal site, and a very weak one at 1860 cm^{-1}. IR spectra of CO adsorbed on some Pd core–Pt shell bimetallic nanoparticles are collected in Fig. 21. Strong bands are found at 2062–2068 cm^{-1} for various metal compositions, which indicates these bimetallic nanoparticles have Pt atoms on the surface. The peak derived from CO adsorbed on Pd at 1941 cm^{-1} can only be found for the bimetallic nanoparticles at the ratio of Pd : Pt = 1 : 4. In contrast, as shown in Fig. 22(*a*), the IR spectra of CO adsorbed on Pt core–Pd shell (1 : 2) bimetallic nanoparticles prepared by successive reduction are totally different from the spectra shown in Fig. 21. This spectrum is almost the same as that of Pd monometallic nanoparticles shown in Fig. 20(*a*), as expected. The amount of Pd atoms needed to cover the Pt core with a monolayer of Pd atoms is about 1.7 times that of Pt, which can be calculated from the Pt core particle size (≈1.5 nm). So the average thickness of the Pd shell on the Pt core is about one layer, which corresponds to the particle size (≈2.3 nm).

4.1.2 PVP-stabilized Au–Pd and Au–Pt bimetallic nanoparticles. PVP-stabilized Au–Pd[137] and Au–Pt[98,138] bimetallic nanoparticles were prepared by alcohol co-reduction. The colloidal dispersions of Au–Pd and Au–Pt bimetallic nanoparticles by simultaneous reduction can be examined by UV/VIS spectra and transmission electron microscopy.[26,32,80]

Comparison of the UV/VIS spectra of the physical mixtures of the corresponding two monometallic nanoparticles with those of PVP-stabilized Au–Pd and Au–Pt bimetallic nanoparticles clearly indicates the formation of new bimetallic species (Fig. 23 and 24), thanks to the strong absorption peak in the red region of Au nanoparticles. Fig. 25 shows the relationship of the peak area of the plasmon absorption of Au monometallic and Au–Pt bimetallic nanoparticle dispersions with the mole ratio of Au in the systems. The PVP-stabilized Au–Pt bimetallic nanoparticle dispersions have a much smaller peak area than the physical mixture of the Au and Pt

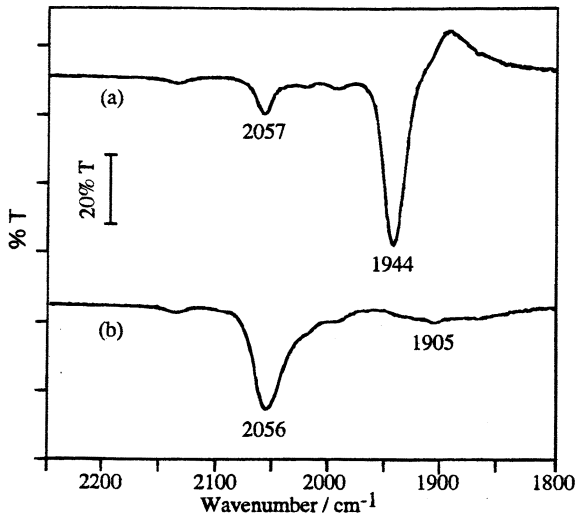

Fig. 22 FTIR spectra of CO adsorbed on PVP-stabilized Pt core–Pd shell bimetallic nanoparticles: (*a*) Pt–Pd (1 : 2), (*b*) Pt–Pd (4 : 1) (co-reduction). [Pt] = 1.0×10^{-4} mol in 10 cm^3 of CH_2Cl_2. (Reprinted with permission from ref. 106. Copyright 1997 American Chemical Society)

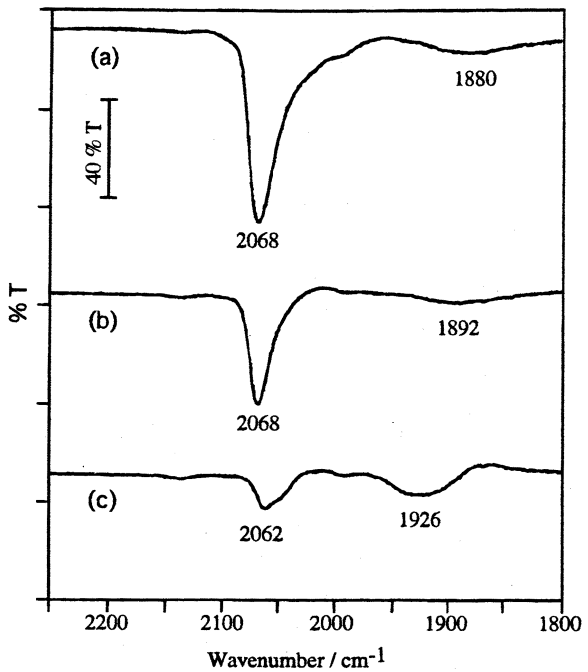

Fig. 21 FTIR spectra of CO adsorbed on PVP-stabilized Pd core–Pt shell bimetallic nanoparticles: (*a*) Pt–Pd (2 : 1), (*b*) Pt–Pd (1 : 1), (*c*) Pt–Pd (1 : 4). [Pd] = 1.0×10^{-4} mol in 10 cm^3 of CH_2Cl_2. (Reprinted with permission from ref. 106. Copyright 1997 American Chemical Society)

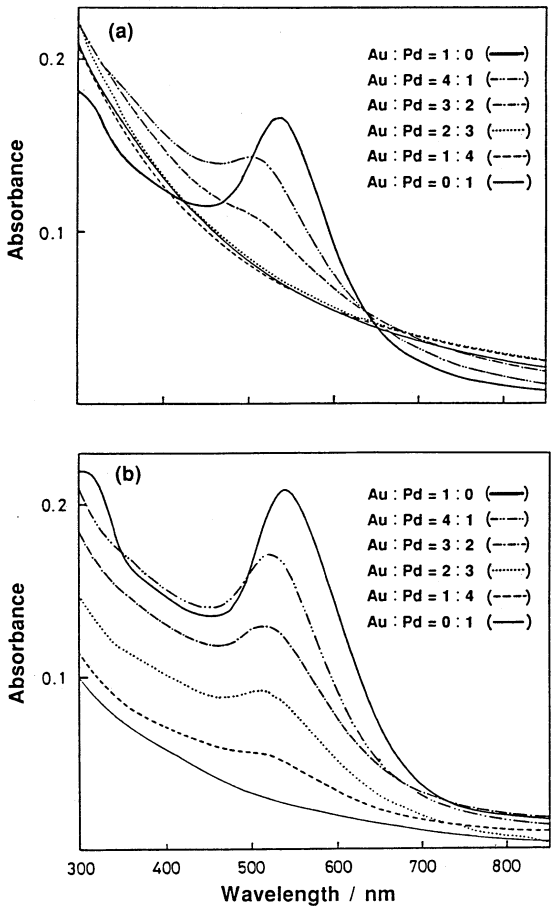

Fig. 23 UV/VIS spectra of (*a*) colloidal dispersions of PVP-stabilized Au–Pd bimetallic nanoparticles and (*b*) physical mixtures of colloidal dispersions of PVP-stabilized Au and Pd monometallic nanoparticles, at various Au:Pd ratios. (Reprinted with permission from ref. 137. Copyright 1992 American Chemical Society)

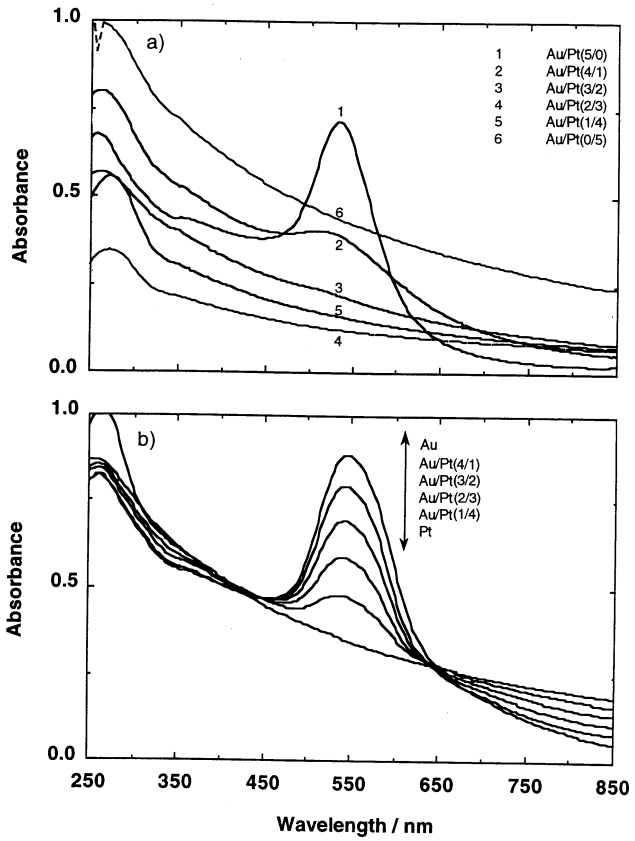

Fig. 24 UV/VIS spectra of (*a*) colloidal dispersions of PVP-stabilized Au–Pt bimetallic nanoparticles and (*b*) physical mixtures of colloidal dispersions of PVP-stabilized Au and Pt monometallic nanoparticles, at various Au : Pd ratios. (Adapted from ref. 138. Copyright 1992 Wiley-VCH Verlag)

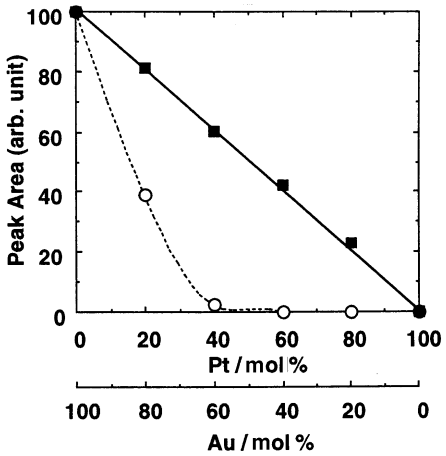

Fig. 25 Relationship between the metal molar ratio and the area of the plasmon absorption peak in (○) PVP-stabilized Au–Pt bimetallic nanoparticles and (■) physical mixture of PVP-stabilized Au and Pt monometallic nanoparticles. (Adapted from ref. 138. Copyright 1992 Wiley-VCH Verlag)

nanoparticle dispersions at the same ratio. This fact indicates that each Au–Pt bimetallic nanoparticle has such a structure that at least both Au and Pt atoms bind to each other in a particle. Similar observations of the color change from red to brown were also reported recently by Schmid's group, in the Pt shell–Au core bimetallic nanoparticles prepared by a successive reduction procedure.[57]

Fig. 13 and 14 show the XRD spectra of the PVP-stabilized monometallic nanoparticles, the 1 : 1 (mole ratio) bimetallic nanoparticles and the physical mixtures of 1 : 1 (mole ratio) of the two kinds of monometallic nanoparticles. Between the XRD spectrum of Au–Pd bimetallic nanoparticles and that of the physical mixture of the two corresponding monometallic nanoparticles, the difference is clear. As shown in Fig. 13(*c*), Au monometallic nanoparticles have sharp peaks suggesting that they are well-crystallized, consistent with the TEM observation that Au nanoparticles are large and geometrically regular. The XRD pattern of the physical mixture of Au and Pd nanoparticles contains both the narrow reflections and much broader peaks, corresponding to Au and Pd nanoparticles, respectively. The peaks found in the spectrum of the Au–Pd bimetallic nanoparticles are not sharp but resemble those in the spectrum of Pd–Pt bimetallic nanoparticles. The principal reason is heterogeneous bond formation in bimetallic nanoparticles. The size of the particles also affects the broadness of the peaks.

The XRD pattern of a physical mixture of Au and Pt nanoparticles shows four sharp peaks corresponding to Au nanoparticles and Pt nanoparticles. In contrast, the XRD pattern of the Au–Pt bimetallic nanoparticles has only two broad peaks, indicating the formation of new bimetallic crystalline species.

The comparison of the XRD patterns of physical mixtures of monometallic nanoparticles with those of bimetallic ones clearly demonstrates that each particle has both metals in it and involves three kinds of metal bonds: two homometal bonds (bond between the same element) and one heterometal bond (bond between different elements).

Quantitative XPS data shown in Table 2 also suggest these bimetallic nanoparticles have Au core–Pd shell and Au core–Pt shell structures. To consider the detailed structure of these bimetallic nanoparticles, EXAFS measurements were carried out on PVP-stabilized Au–Pd bimetallic nanoparticles as well as on Pd–Pt ones. For Au–Pt bimetallic nanoparticles, EXAFS is difficult to apply because of the similarity in energy of the X-ray absorption edges.

The EXAFS data for Au–Pd (1 : 4) bimetallic nanoparticles are collected in Table 6. The sum of the observed coordination numbers around Pd and Au is 5.4 and 10.7, respectively, which suggests Au atoms are located preferentially in an inner core. From TEM observation, Au–Pd (1 : 4) bimetallic nanoparticles have an average diameter of 1.6 nm. Therefore, the Au–Pd (1 : 4) bimetallic nanoparticles consist of centered 6 atoms and the 2-atomic layered atoms with an fcc structure around the 6 atoms, and total 110 atoms, as shown in Fig. 26. The coordination numbers calculated on the basis of an Au core–Pd shell structure are quite close to the

Table 6 Coordination numbers around the Pd and Au atoms in an Au–Pd (1 : 4) bimetallic cluster determined by a simultaneous fitting and those calculated for the models[a]

Absorbing metal	Scattering metal	Interatomic distance r/Å	Coordination number N		
			Obsd	Au core[b]	Random[b]
Pd	Pd	2.77 ± 0.03	4.2 ± 0.8	6.4	6.9
Pd	Au	2.78 ± 0.03	1.2 ± 0.3	1.4	1.7
Au	Au	2.82 ± 0.03	6.2 ± 1.9	6.3	1.7
Au	Pd	2.78 ± 0.03	4.5 ± 1.1	5.7	6.9

[a] Reprinted with permission from ref. 137. Copyright 1992 American Chemical Society. [b] See Fig. 26.

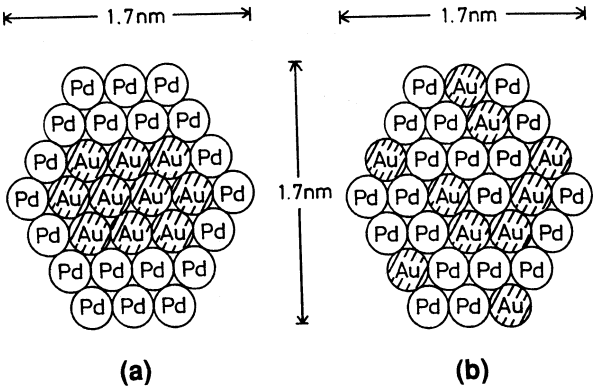

Fig. 26 Cross-sections of models for PVP-stabilized Au–Pd (1 : 4) bimetallic nanoparticles: (*a*) Au core–Pd shell model, (*b*) random model. (Reprinted with permission from ref. 137. Copyright 1992 American Chemical Society)

observed value, as shown in Table 6. Thus, one can take this core–shell structure as a model for the Au–Pd (1 : 4) bimetallic nanoparticles. In the case of Au–Pd (1 : 1) bimetallic nanoparticles, the model construction may be difficult due to the large size. The observed coordination numbers can suggest two models (Table 7), one is the Au single-core model [Fig. 27(*a*)] and the other is the 'cluster-in-cluster' model [Fig. 27(*b*)]. In this case the cluster-in-cluster model is the best. We will discuss later on bimetallic nanoparticles with the cluster-in-cluster structure.

4.1.3 Other bimetallic nanoparticles with core–shell structure. Pt–Rh bimetallic nanoparticles could also be prepared by the alcohol co-reduction procedure.[115] In Table 8, the coordination numbers obtained by EXAFS and calculated from two models are collected. From TEM observation, the average diameter of Pt–Rh bimetallic nanoparticles is 4.0 nm. However, detailed observation with HRTEM revealed that these particles contain smaller nanoclusters with a diameter of 0.8–1.5 nm, which corresponds to the small coordination numbers obtained by EXAFS. From EXAFS data, each nanocluster is calculated to have a modified core–shell structure as shown in Fig. 28. A whole particle of Pt–Rh (1 : 1) bimetallic nanoparticles can be illustrated as shown in Fig. 29.

Co-reduction of two kinds of precious metal ions in refluxing alcohol in the presence of PVP usually gives colloidal dispersions of bimetallic nanoparticles with the core–shell structure. The tendency of metals to occupy the shell is in the following order: Au < Pt < Pd < Rh and the tendency of metals to occupy the core is the reverse. Bimetallic nanoparticles with the core–shell structure can be prepared only under mild reduction conditions in the presence of PVP.

4.1.4 Formation mechanism of bimetallic nanoparticles with core–shell structure. The formation process of bimetallic nanoparticles is essential information for the preparation and design of bimetallic nanoparticles. The formation process may clarify the reason for the special structure formed by simple reduction and, especially, co-reduction of two metal salts.

As described above, however, Pd–Pt, Au–Pd, Au–Pt and Pt–Rh bimetallic nanoparticles prepared by *simultaneous*

Table 7 Coordination numbers around the Pd and Au atoms in an Au–Pd (1 : 1) bimetallic cluster determined by a simultaneous fitting and those calculated for the models[a]

Absorbing metal	Scattering metal	Interatomic distance r/Å	Coordination number N			
			Obsd	Au core[b]	Cluster-in-cluster[b]	Random[b]
Pd	Pd	2.78 ± 0.03	1.5 ± 0.3	4.1	6.3	4.7
Pd	Au	2.78 ± 0.03	2.5 ± 0.4	3.2	2.6	4.7
Au	Au	2.82 ± 0.03	6.5 ± 1.5	8.4	7.3	4.7
Au	Pd	2.78 ± 0.03	2.3 ± 0.4	3.1	2.6	4.7

[a] Reprinted with permission from ref. 137. Copyright 1992 American Chemical Society. [b] See Fig. 27.

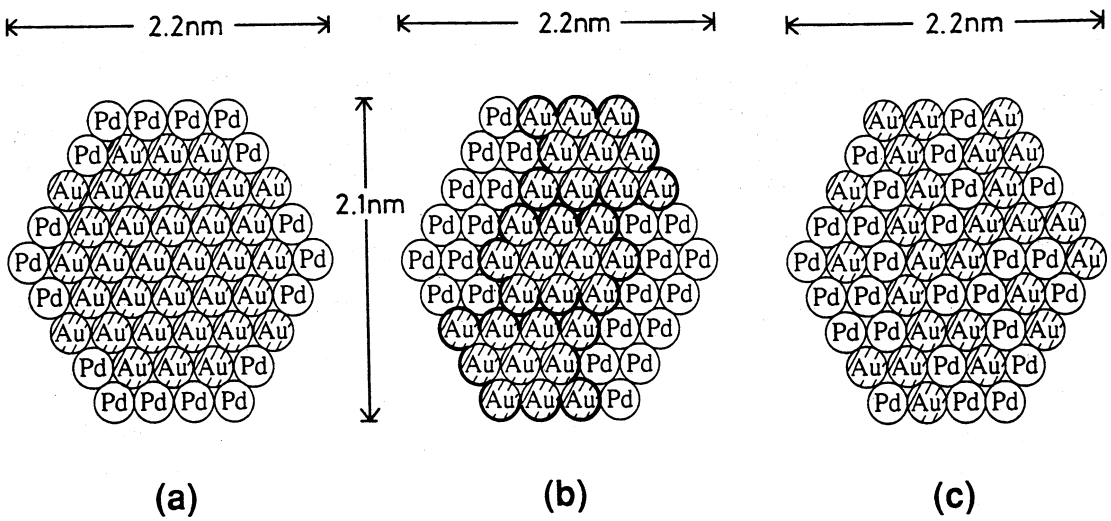

Fig. 27 Cross-sections of models for PVP-stabilized Au–Pd (1 : 1) bimetallic nanoparticles: (*a*) Au single-core–Pd shell model, (*b*) cluster-in-cluster model, (*c*) random model. (Reprinted with permission from ref. 137. Copyright 1992 American Chemical Society)

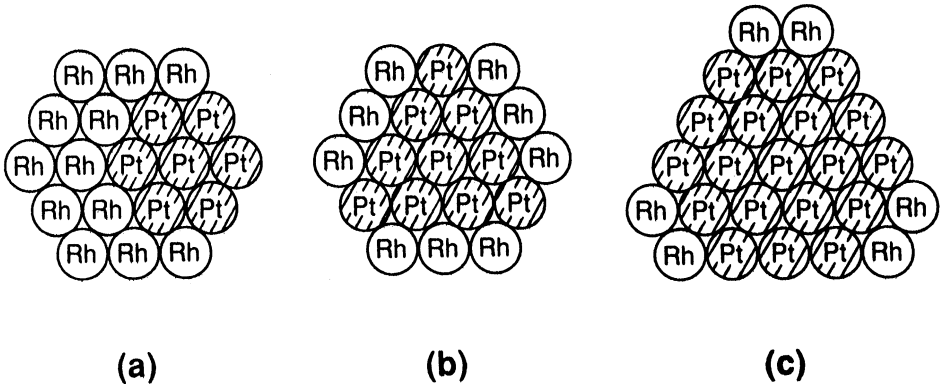

Fig. 28 Cross-sections of models for (*a*) Pt–Rh (1 : 4) bimetallic sub-nanoparticle, (*b*) Pt–Rh (1 : 1) bimetallic sub-nanoparticle and (*c*) Pt–Rh (4 : 1) bimetallic sub-nanoparticle. (Reprinted with permission from ref. 115. Copyright 1994 American Chemical Society)

Table 8 Coordination numbers of PVP-stabilized Pt–Rh (1 : 1) bimetallic nanoparticles determined from EXAFS data and those calculated for the models[a]

			Coordination number *N*		
Sample	Edge	Bond	Obsd	Pt core	Random
Pt–Rh (1 : 1)	Rh K	Rh—Rh	2.6 ± 0.5	3.1	3.9
		Rh—Pt	3.1 ± 0.8	3.0	3.9
	Pt L_3	Pt—Pt	6.3 ± 1.0	6.6	3.9
		Pt—Rh	1.7 ± 0.8	2.9	3.9

[a] Reprinted with permission from ref. 115. Copyright 1994 American Chemical Society.

alcohol reduction have core–shell structures. To reveal the formation process of the core–shell structure by simultaneous reduction, UV/VIS spectral changes were investigated during the reduction of metal ions and the growth of metal nanoparticles. We take Au–Pd bimetallic nanoparticles as an example here. Fig. 30 shows the spectral changes observed during the heating of a solution of $HAuCl_4$ and the mixture of $HAuCl_4$ and $PdCl_2$ to 30 °C in the presence of PVP. During the first 1500 s $[AuCl_4]^-$ (identified with the absorption peak at *ca.* 320 nm) was reduced, followed by the reduction of Pd^{II}. After the reduction of $[AuCl_4]^-$, a weak, broad peak attributed to the plasmon absorption of Au clusters appears at *ca.* 550 nm, indicating that the aggregation of Au atoms occurs. This reduction order can be explained by the redox potentials of metal ions (collected in Table 9). In addition, comparing the curves in Fig. 31, one can clearly see that the reduction of $[AuCl_4]^-$ is accelerated by addition of Pd^{II}. These results clearly indicate that Pd^{II} can act as an 'electron-mediating' catalyst for the reduction of $[AuCl_4]^-$. The reduction process of the two metal ions is a 'geared step-cycled reduction', as shown in Scheme 1. The formation process of Pd–Pt bimetallic nanoparticles can also be interpreted by Scheme 2.

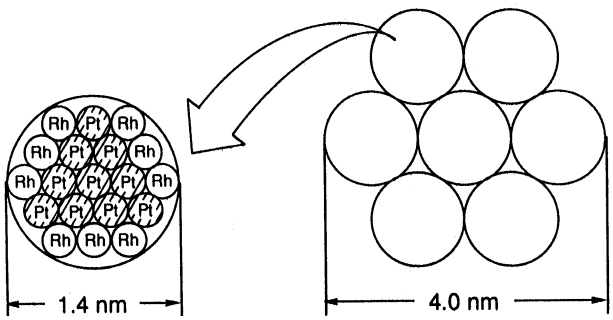

Fig. 29 Cross-section of the assembly model of a PVP-stabilized Pt–Rh (1 : 1) bimetallic sub-nanoparticle. (Reprinted with permission from ref. 115. Copyright 1994 American Chemical Society)

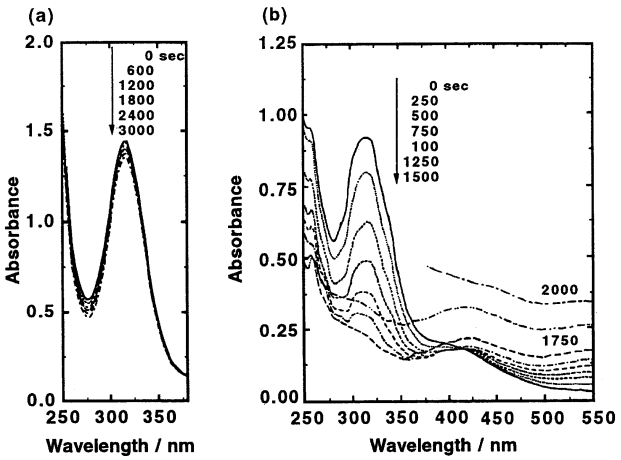

Fig. 30 UV/VIS spectral change during the reduction of (*a*) $HAuCl_4$ and (*b*) $PdCl_2$–$HAuCl_4$ (1 : 1) in ethanol–water (1 : 1) in the presence of PVP at 30 °C. $[Au] = 6.6 \times 10^{-4}$ mol dm^{-3} in a 10 mm cell. (Reprinted with permission from ref. 117. Copyright 1995 Royal Society of Chemistry)

In the case of a mixture of $[PtCl_6]^{2-}$ and $[AuCl_4]^-$, the reduction processes are slightly different from that of the mixtures containing Pd^{II}. The UV/VIS spectral change during the reduction of $[AuCl_4]^-$ in the $[AuCl_4]^-$–$[PtCl_6]^{2-}$ mixture indicates that $[AuCl_4]^-$ is reduced earlier than $[PtCl_6]^{2-}$, as can be understood from a consideration of the redox potentials of the two metal ions. As distinct from the cases of Pd–Pt and Au–Pd, the reduction rate of $[AuCl_4]^-$ in the Au–Pt mixed solution is a little slower than in a monometallic $[AuCl_4]^-$ solution (Fig. 32). These situations can also be explained by a geared step-cycled reduction as shown in Scheme 3.

In this process, stabilizing polymers play an important role. Stabilizing polymers such as PVP and PVA can coordinate to metal ions before the reduction. Thanks to this complex formation, the metal ions can be reduced so smoothly under mild

Table 9 Some redox reactions related to the formation of precious metal nanoparticles and their redox potentials

Reaction	Redox potential /V *vs.* NHE[a]
$CH_3CH_2OH \rightarrow CH_3CHO + 2\,H^+ + 2\,e^-$	−0.16
$Pd^{2+} + 2\,e^- \rightarrow Pd$	0.99
$Pd(OH)_2 + 2\,e^- \rightarrow Pd$	0.07
$PtCl_6^{2-} + 2\,e^- \rightarrow PtCl_4^{2-} + 2\,Cl^-$	0.68
$PtCl_4^{2-} + 2\,e^- \rightarrow Pt + 4\,Cl^-$	0.73
$AuCl_4^- + 3\,e^- \rightarrow Au + 4\,Cl^-$	1.00

[a] NHE = normal hydrogen electrode.

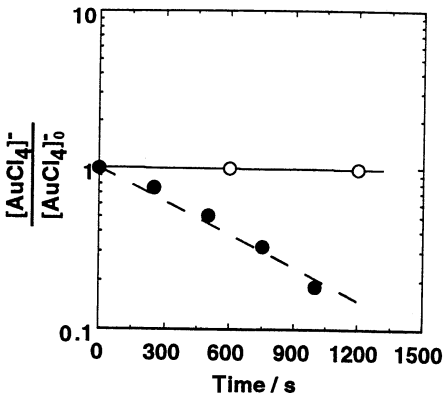

Fig. 31 Temporal dependence of the rate of $HAuCl_4$ reduction during heating of (○) an ethanol–water (1 : 1) solution of $HAuCl_4$ and (●) a 1 : 1 mixture of $HAuCl_4$ and $PdCl_2$ at 30 °C in the presence of PVP. (Reprinted with permission from ref. 117. Copyright 1995 Royal Society of Chemistry)

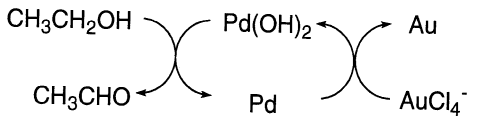

Scheme 1

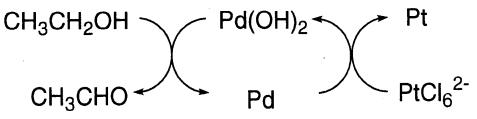

Scheme 2

conditions that the obtained nanoparticles have smaller size and narrower size distributions than the conventional colloids obtained without PVP as described above.

Stabilizing polymers play another important role to control the particle structure, besides the formation of the polymer–metal *ion* complex. The order of the reduction of the two metal components is controlled by their redox potentials. Afterwards, the interaction between zerovalent metal atoms and stabilizing polymers is also of great importance. In fact,

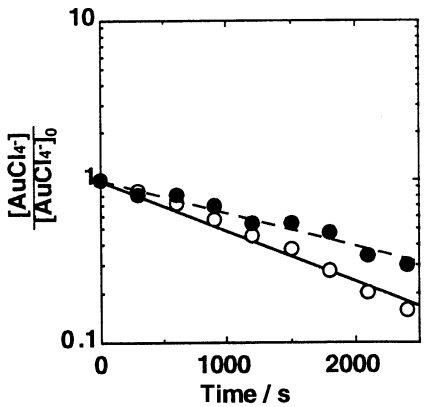

Fig. 32 Temporal dependence of the rate of $HAuCl_4$ reduction during heating of (○) an ethanol–water (1 : 1) solution of $HAuCl_4$ and (●) a 1 : 1 mixture of $HAuCl_4$ and H_2PtCl_6 at 70 °C in the presence of PVP. (Reprinted with permission from ref. 117. Copyright 1995 Royal Society of Chemistry)

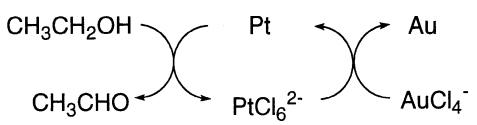

Scheme 3

without the stabilizing polymer, it is difficult to construct the core–shell structure.

As proposed in Fig. 33,[117] the metal ions coordinate to the stabilizing polymer at first, giving a polymer–metal *ion* complex. Then, ions of one of the two metal elements, having the higher redox potential, are reduced. After that, the ions of the other metal element are reduced and then the firstly reduced zerovalent metal atoms, which are more weakly coordinated with the polymer than the other metal atoms, start to aggregate to form pre-nanoparticles. In this process, zerovalent metal atoms coordinate to the stabilizing polymer and form a 'polymer–metal *atom* complex'. The aggregated metal atoms form pre-nanoparticles, which also coordinate to the stabilizing polymer, forming a 'polymer–metal *nanoparticle* complex', in other words, polymer-stabilized metal nanoparticles. In the same polymer, the secondly reduced metal atoms are coordinated. Then, they deposit onto the pre-nanoparticles of the first reduced metal to generate core–shell structured bimetallic nanoparticles.

4.2 Cluster-in-cluster structure

In the bimetallic nanoparticles with cluster-in-cluster structures, one element forms nanoclusters and the other element surrounds the nanoclusters and acts as a binder. The cluster-in-cluster structure may be considered as a modification of the core–shell structure.

In the case of Au–Pd (1 : 1) bimetallic nanoparticles prepared by co-reduction of both metal ions by alcohol in the presence of PVP, the cluster-in-cluster structure is supported by EXAFS data. The EXAFS data and some possible models are shown in Table 7 and Fig. 27, respectively. Based on the consistency in the coordination numbers, the cluster-in-cluster structure has been chosen.

Schmid *et al.*[57] reported Pd core–Au shell and Au core–Pd shell bimetallic nanoparticles prepared by a successive reduction process. However, by successive alcohol reduction of $PdCl_2$ and $AuCl_4^-$ one cannot always obtain homogeneous bimetallic nanoparticles. The relationship between the reduction process and the structure of PVP-stabilized Au–Pd bimetallic nanoparticles is summarized in Table 10. The successive reduction, starting from the preparation of Au pre-nanoparticles (Au then Pd), could provide only a mixture of the monometallic clusters of both elements. In contrast, the reverse successive reduction, starting from the preparation of Pd pre-nanoparticles (Pd then Au), could provide the cluster-in-cluster structure having '2 Au cores' as shown in Fig. 34. This structure can be interpreted by the so-called geared step-cycled reduction, which was explained in the previous section.

The Pd–Pt bimetallic nanoparticles were supported on an inorganic support and treated by heat, in order to apply the bimetallic nanoparticles to the heterogeneous catalyst. The structure of the supported Pd–Pt bimetallic nanoparticles was analyzed by EXAFS, revealing that the bimetallic nanoparticles have the cluster-in-cluster structure.[139] This change of structure from core–shell to cluster-in-cluster could be performed by coagulation and atomic re-arrangement of the

Table 10 Relation between the reduction procedure and the structure of Au–Pd bimetallic nanoparticles[a]

	Structure	
Reduction procedure	Au–Pd (1 : 4)	Au–Pd (1 : 1)
Successive (Pd then Au)	2 Au cores	Cluster-in-cluster
Successive (Au then Pd)	Mixture	Mixture
Co-reduction	Au core	Cluster-in-cluster

[a] Reprinted with permission from ref. 102. Copyright 1993 American Chemical Society.

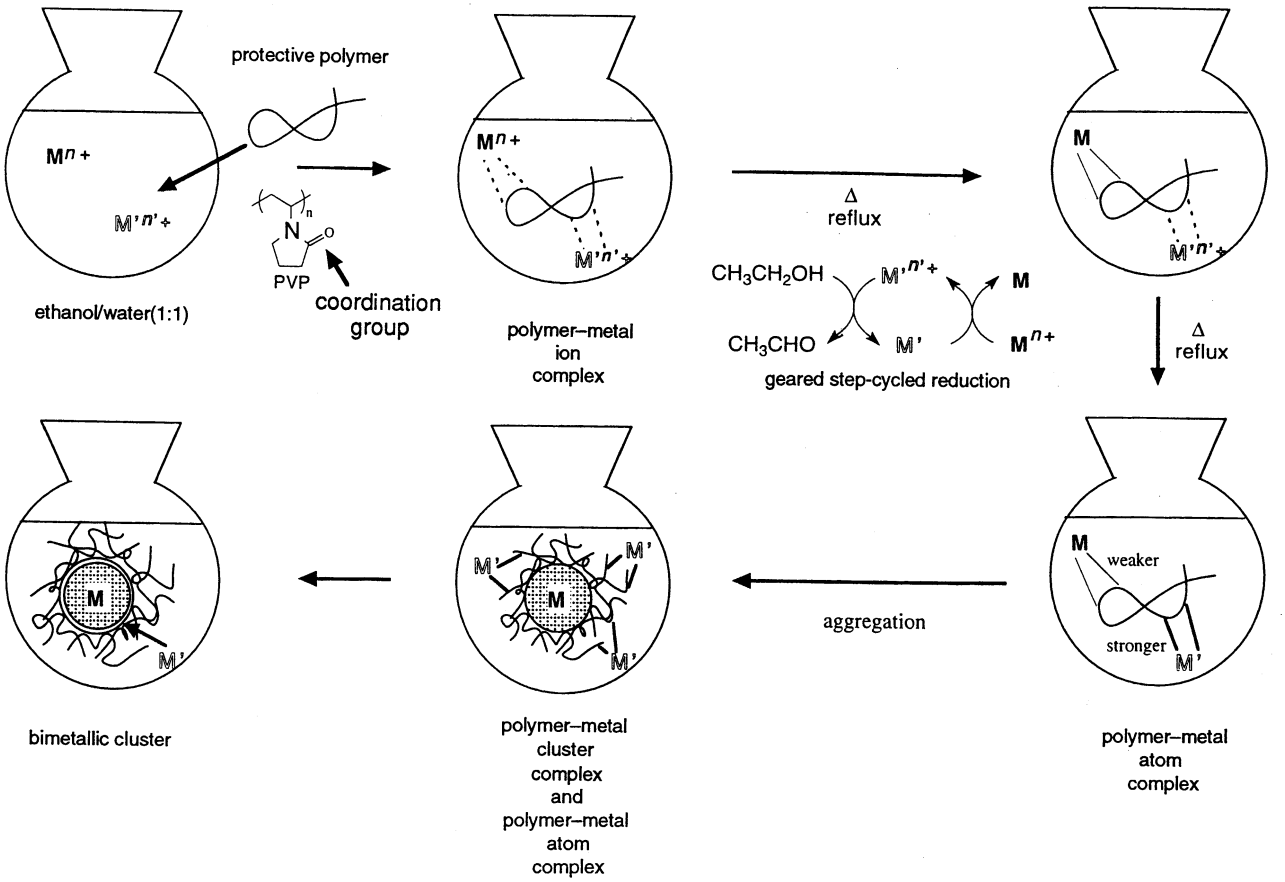

Fig. 33 Proposed formation mechanism of polymer-stabilized noble bimetallic nanoparticles prepared by alcohol reduction in the presence of PVP. (Reprinted with permission from ref. 117. Copyright 1995 Royal Society of Chemistry)

nanoparticles. This is consistent with the idea that the cluster-in-cluster structure is a modification of the core–shell structure.

4.3 Alloy structure

In bulk metals, two kinds of metal elements often provide an alloy structure. If the atomic sizes of two elements are similar to each other, then it will be a random alloy. When the atom sizes are quite different from each other and the mole ratio of the two elements is simple and adequate to the structure, then they form an intermetallic compound. In the case of bimetallic nanoparticles, these kinds of alloy structures seem to be more easily produced than in the case of bulk metals. In fact, we have found that bimetallic nanoparticles between precious metals and light transition metals have such alloy structures.

PVP-stabilized Cu–Pd[86–88] and Ni–Pd[89] bimetallic nanoparticles can be prepared by a modified alcohol co-reduction using ethylene glycol as the solvent-reductant. In the case of Cu–Pd bimetallic nanoparticles, UV/VIS spectroscopy gives good information. As shown in Fig. 35, a plasmon absorption peak at *ca.* 560 nm is found in the spectrum of the Cu monometallic nanoparticle dispersion. However, the spectrum of the dispersion of PVP-stabilized Cu–Pd (2 : 1) bimetallic nanoparticles is monotonic and shows no absorption peak, suggesting the formation of alloyed bimetallic nanoparticles. The formation of a bimetallic alloy phase in Cu–Pd bimetallic nanoparticles was clearly evident from the XRD patterns, as shown in Fig. 36. The star-marked lines are due to sodium sulfate. The pattern of Cu–Pd bimetallic nanoparticles exhibits diffraction lines at $2\theta = 42.0°$, 48.4°, 72.0° and 87.0°, which are located between the corresponding diffraction peaks of the two corresponding monometallic nanoparticles. This strongly suggests

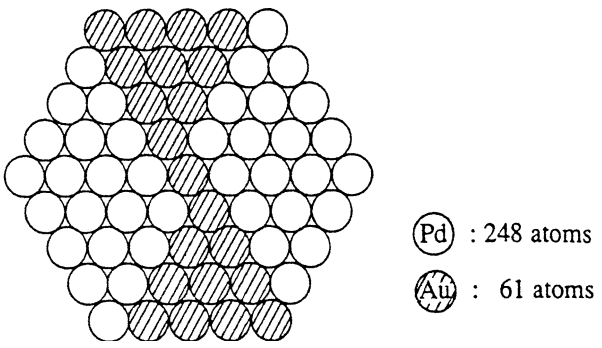

Fig. 34 Cross-section of a model for PVP-stabilized Au–Pd (1 : 4) bimetallic nanoparticles prepared by successive reduction (Pd then Au). (Reprinted with permission from ref. 102. Copyright 1993 American Chemical Society)

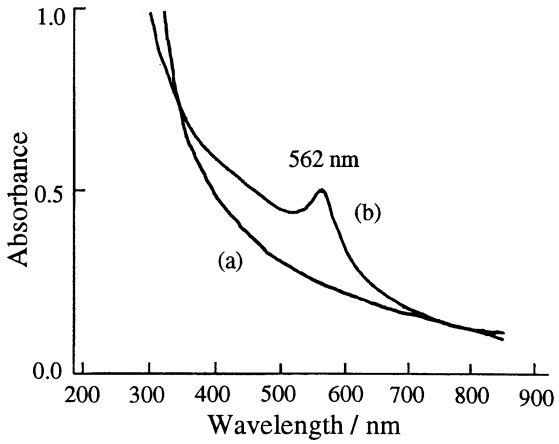

Fig. 35 UV/VIS spectra of (*a*) PVP-stabilized Cu–Pd (2 : 1) bimetallic nanoparticles and (*b*) Cu monometallic nanoparticles. (Reprinted with permission from ref. 86. Copyright 1993 The Chemical Society of Japan)

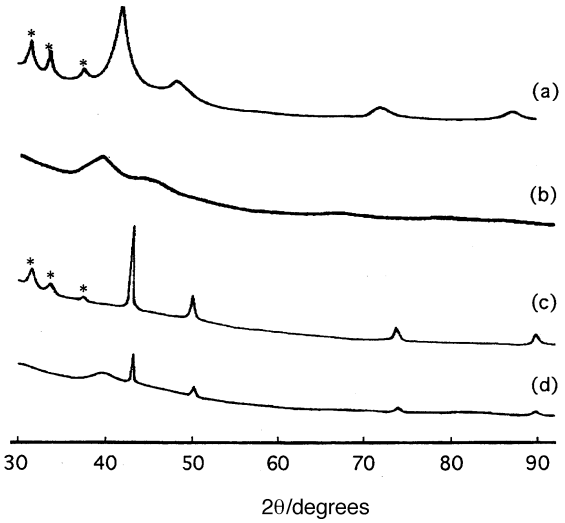

Fig. 36 X-Ray diffractograms of (*a*) PVP-stabilized Cu–Pd (2 : 1) bimetallic nanoparticles, (*b*) PVP-stabilized Pd nanoparticles, (*c*) PVP-stabilized Cu nanoparticles and (*d*) physical mixture of dispersions (*b*) and (*c*) with Cu : Pd = 2 : 1. (Reprinted with permission from ref. 86. Copyright 1993 The Chemical Society of Japan)

formation of an alloy structure. The catalytic properties of the Cu–Pd bimetallic nanoparticles are consistent with the alloy structure. As will be mentioned in the next section, the Cu–Pd bimetallic nanoparticles work as catalysts both for the hydrogenation of dienes (Pd-catalyzed reaction) and the hydration of nitriles (Cu-catalyzed reaction). A similar XRD analysis was carried out with Ni–Pd bimetallic nanoparticles.

5 Catalytic Properties

Catalysis is the most important chemical application of metal nanoparticles and has been extensively studied. Transition metals, especially precious metals, show very high catalytic abilities for many organic reactions. Moreover, the colloidal dispersions of metal nanoparticles can be used as photocatalysts, because these dispersions are normally transparent to light. In this chapter, homogeneous bimetallic nanoparticle catalysts will be mainly discussed. Immobilization of nanoparticles to prepare heterogeneous catalysts has been investigated as well, but this subject will be treated elsewhere.

5.1 Hydrogenation of olefins

Polymer (such as PVP or PVA)-stabilized Pd, Pt, Rh and Ir nanoparticles prepared by alcohol reduction were used as effective hydrogenation catalysts for many unsaturated olefins.[49,73,74] In particular, Pd nanoparticles were used as a selective catalyst for the partial hydrogenation of dienes to monoenes with very high activity and selectivity.

Bimetallic nanoparticles including Pd were also applied to this kind of hydrogenation catalysts. PVP-stabilized Pd–Pt[82,83] and Au–Pd[137] bimetallic nanoparticles with various metal compositions were used as catalysts for the selective hydrogenation of 1,3-cyclooctadiene to cyclooctene. In both cases, the bimetallic nanoparticles with a Pd content of 80% showed the highest activity, which is greater than Pd nanoparticles themselves (Fig. 37 and 38). As described above, EXAFS analyses of these bimetallic nanoparticles indicated that they have Pt or Au core–Pd shell structures. Furthermore, from the particle sizes, at 80% Pd the particles are fully covered by Pd atoms [Fig. 16(*a*)[81,116] and 26(*a*)[137]]. This improvement of activity shall be interpreted only by a ligand effect.

Detailed consideration of catalytic activity and selectivity was done in the case of Pd–Pt bimetallic nanoparticles.[83] Firstly, in order to avoid any interactions with hydrogen, PVP-stabilized Pd–Pt nanoparticles were prepared and stored

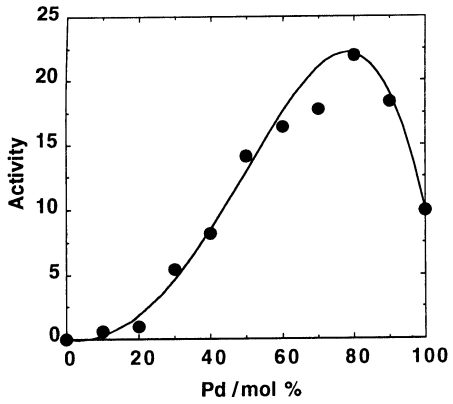

Fig. 37 Relationship between catalytic activity [in mmol H_2 per mmol (Pd + Pt) per s] and metal composition of colloidal dispersions of PVP-stabilized Pd–Pt bimetallic nanoparticles, prepared by co-reduction under ambient air conditions, for the hydrogenation of 1,3-cyclooctadiene. [1,3-COD] = 2.5×10^{-2} mol dm^{-3}, [catalyst] = 1.0×10^{-5} mol dm^{-3}, ethanol solvent at 30 °C, $p(H_2)$ = 1 atm. (Reprinted with permission from ref. 83. Copyright 1993 Royal Society of Chemistry)

under nitrogen and used as the catalyst for the same reaction. The catalytic activity was slightly lower than for those prepared and stored under air (Fig. 39), but Pd–Pt (4 : 1) nanoparticles are again the most active catalyst. This strongly suggests that the structure of bimetallic Pd–Pt nanoparticles may have an affect on the catalytic activity.

In order to examine the effect of the surface area of the catalyst, the catalytic activity was normalized by the surface area, calculated from the average diameters of the nanoparticles measured by TEM. The dependence of normalized activity on the metal composition has again a similar shape to that of the apparent activity. Since Pd has a high catalytic activity for hydrogenation of diene and Pt has a low one, the selective existence of Pd atoms on the surface of bimetallic nanoparticles (suggested by EXAFS results) may account for the high catalytic activity. The catalytic activity of a Pd atom on the surface of bimetallic nanoparticles was calculated. Fig. 40 shows the relationship between the metal composition of the Pd–Pt bimetallic nanoparticles and the catalytic activity of the surface Pd atom. The activity of surface Pd atoms is almost constant for bimetallic nanoparticles containing between

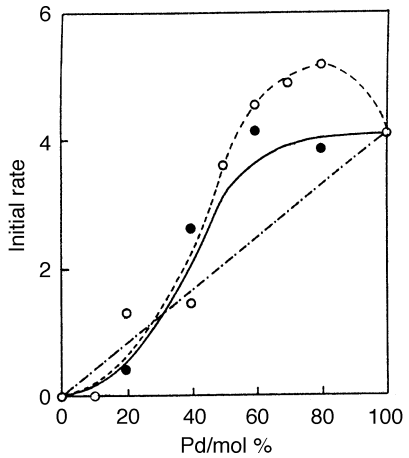

Fig. 38 Relationship between catalytic activity [in mmol H_2 per mmol (Au + Pd) per s] and metal composition of (○) colloidal dispersions of PVP-stabilized Au–Pd bimetallic nanoparticles prepared by co-reduction under ambient air conditions and (●) a mixture of Au and Pd monometallic nanoparticles, for the hydrogenation of 1,3-cyclooctadiene. [1,3-COD] = 2.5×10^{-2} mol dm^{-3}, [catalyst] = 1.0×10^{-5} mol dm^{-3}, ethanol solvent at 30 °C, $p(H_2)$ = 1 atm. (Reprinted with permission from ref. 129. Copyright 1992 American Chemical Society)

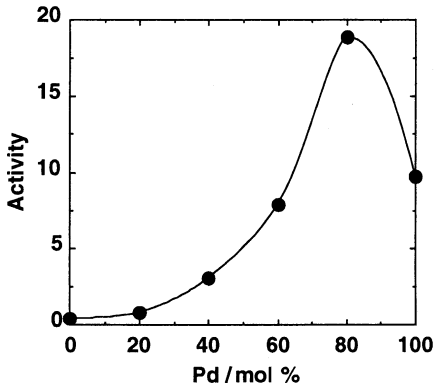

Fig. 39 Relationship between catalytic activity [in mmol H_2 per mmol (Pd + Pt) per s] and metal composition of colloidal dispersions of PVP-stabilized Pd–Pt bimetallic nanoparticles prepared by co-reduction under nitrogen gas for the hydrogenation of 1,3-cyclo-octadiene. [1,3-COD] = 2.5×10^{-2} mol dm^{-3}, [catalyst] = 1.0×10^{-5} mol dm^{-3}, ethanol solvent at 30 °C, $p(H_2) = 1$ atm. (Reprinted with permission from ref. 83. Copyright 1993 Royal Society of Chemistry)

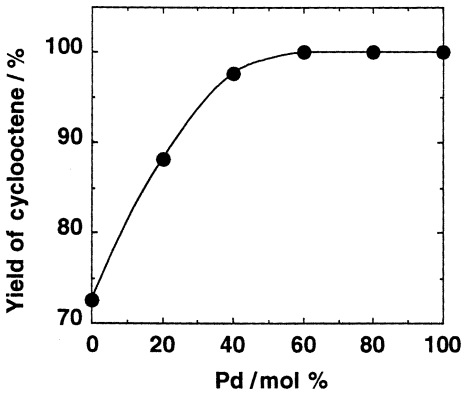

Fig. 41 Dependence on the metal composition of the yield of cyclo-octene from the hydrogenation of 1,3-cyclooctadiene with a PVP-stabilized Pd–Pt bimetallic nanoparticle catalyst. The hydrogenation was carried out until an equimolar amount of hydrogen to 1,3-cyclo-octadiene was consumed. (Reprinted with permission from ref. 83. Copyright 1993 Royal Society of Chemistry)

50–95 mol% of Pd. The normalized activity of surface Pd atoms in the bimetallic nanoparticles is larger than that of monometallic Pd nanoparticles. As the ionic potential of Pd (8.34 eV) is smaller than that of Pt (9.0 eV), the electronic interaction between the Pt core and the surface shell Pd atoms results in the Pd atoms being deficient in electron density. This is a practical example of the ligand effect, since a substrate with C=C bonds favors the electron-deficient catalytic sites. The selectivity of monoene produced by these Pd–Pt or Au–Pd bimetallic nanoparticles was as high as that of Pd monometallic nanoparticles, that is, almost 100% (Fig. 41 in the case of Pd–Pt bimetallic nanoparticles).[83]

PVP-stabilized Pd–Rh bimetallic nanoparticles have also been used as a catalyst for the hydrogenation of *cis*-1,3-cyclopentadiene to cyclopentene.[85] These nanoparticles have a core–shell structure as described above. The catalytic activity depends on the metal composition of the bimetallic nanoparticles, as shown in Fig. 42. The highest activity is obtained at a composition of Pd : Rh = 1 : 2. This high activity was not observed with mixtures of the corresponding two monometallic nanoparticles.

5.2 Hydration of acrylonitrile

PVP-stabilized Cu–Pd bimetallic nanoparticles, prepared in hot ethylene glycol under nitrogen, have a Cu^0 state as described above.[86–88] The selective hydration of acrylonitrile to acrylamide, and the hydrogenation of carbon—carbon double bonds under mild conditions are interesting properties of this light transition metal–precious metal bimetallic nanoparticle. The reaction process of this selective hydration of acrylonitrile is as follows:

$$CH_2{=}CH{-}CN + H_2O \rightarrow CH_2{=}CH{-}CONH_2 \quad (1)$$

The rate of this reaction catalyzed by PVP-stabilized Cu–Pd (2 : 1) bimetallic nanoparticles is about 7 times higher than that of the PVP-stabilized Cu nanoparticles, and the activity depends on the Cu : Pd ratio. The higher the Cu : Pd ratio is, the higher the catalytic activity is within a range of Cu : Pd ratio from 1 to 3. With this catalyst, the reaction product is the amide with nearly 100% selectivity. The acceleration effect of Pd in Cu–Pd bimetallic nanoparticles in this hydration is illustrated in Fig. 43. The coordination of the C=C double bond of acrylonitrile to the Pd site brings the C≡N triple bond close to the Cu active site, which makes the hydration easy. This is a typical example of an ensemble effect.

5.3 Photo-induced hydrogen generation from water

Many studies on artificial photosynthesis have been published[97,98,140,141] and photochemical hydrogen generation from water has received much attention for its potential to convert solar energy into chemical energy.[58,98,138,142–145] Well-dispersed micelle- or polymer-stabilized Pt nanoparticles have also been frequently used as catalysts for visible light-

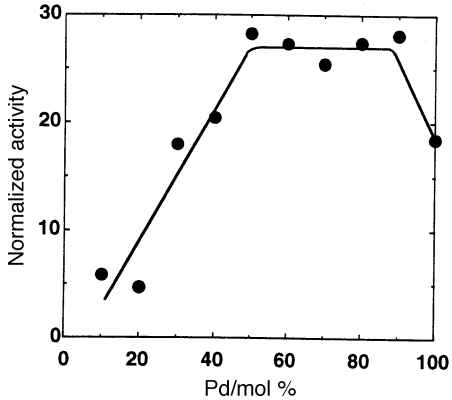

Fig. 40 Normalized catalytic activity (in mmol H_2 per mmol surface Pd per s) as a function of metal composition of PVP-stabilized Pd–Pt bimetallic nanoparticles. The normalization was determined by the number of Pd atoms on the surface of the nanoparticle, assuming that Pd atoms exist selectively on the surface. The original data are the same as in Fig. 37. (Reprinted with permission from ref. 83. Copyright 1993 Royal Society of Chemistry)

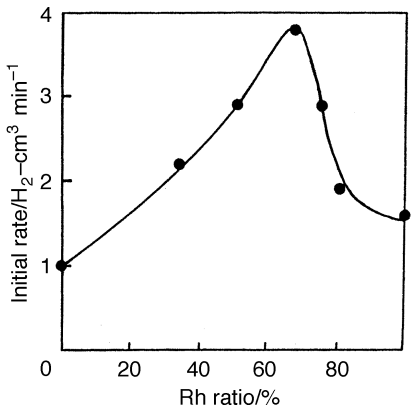

Fig. 42 Dependence on the metal composition of the catalytic activity of PVP-stabilized Pd–Rh bimetallic nanoparticles in the hydrogenation of 1,3-*cis*-cyclopentadiene at 30 °C under 1 atm of hydrogen. (Reprinted with permission from ref. 85. Copyright 1990 Kinki Chemical Society, Japan)

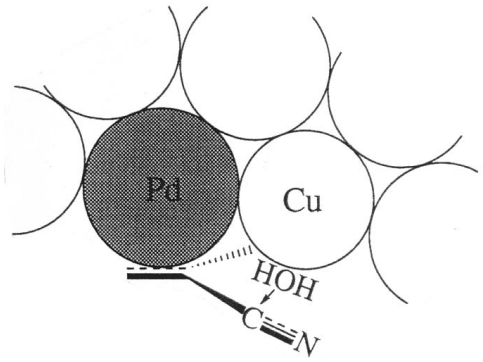

Fig. 43 Schematic diagram of the acceleration effect of Pd in PVP-stabilized Cu–Pd bimetallic nanoparticles on the hydration of acrylonitrile. (Reprinted with permission from ref. 88. Copyright 1994 Wiley-VCH)

induced hydrogen generation with a system such as EDTA–$[Ru(bpy)_3]^{2+}$–methyl viologen–colloidal catalyst (Fig. 44).[143,145,146] Pt nanoparticles stabilized by polymerized micelles are more stable and provide higher activities for visible light-induced hydrogen generation than their polymer-stabilized analogs.

PVP-stabilized Au–Pt bimetallic nanoparticles were applied as a catalyst for this reaction. These bimetallic nanoparticles are considered to have a Au core–Pt shell structure, which may improve the catalytic activity of Pt on the surface. The catalytic activity depends on the metal composition of the Au–Pt bimetallic nanoparticles, as shown in Fig. 45.

The electron transfer from the methyl viologen cation radical to monometallic Pt or Au nanoparticles has been investigated in detail already. These studies indicate that the electron transfer from the methyl viologen cation radical to Au nanoparticles is a diffusion-controlled reaction. However, monometallic Au nanoparticles do not generate hydrogen from water. On the other hand, the rate-determining step of the hydrogen generation catalyzed by Pt is the electron transfer from the methyl viologen cation radical. In the case of PVP-stabilized Au–Pt bimetallic nanoparticles containing both metal elements in each particle, as shown in Fig. 46, the electron transfer from Pt atoms to Au atoms supposedly occurs in the Au–Pt bimetallic nanoparticles. First, the electrons, supplied by the methyl viologen cation radicals, are rapidly transferred to Au atoms and then stored. Then, the stored electrons are transferred to Pt atoms on the surface to generate hydrogen. The co-existence of Au and Pt in a particle may improve the catalytic activity.

PVP-stabilized Pt–Ru bimetallic nanoparticles, prepared by co-reduction, can also be used as catalysts for hydrogen generation from water.[58] Hydrogen generation rate constants (k_{H2}) are summarized in Table 11. They are proportional to the

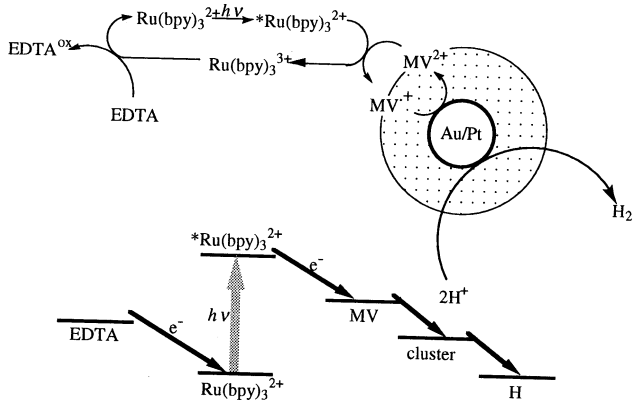

Fig. 44 Schematic illustration of the mechanism of visible light-induced hydrogen generation catalyzed by Au–Pt bimetallic nanoparticles and the electron flow mechanism of the reaction

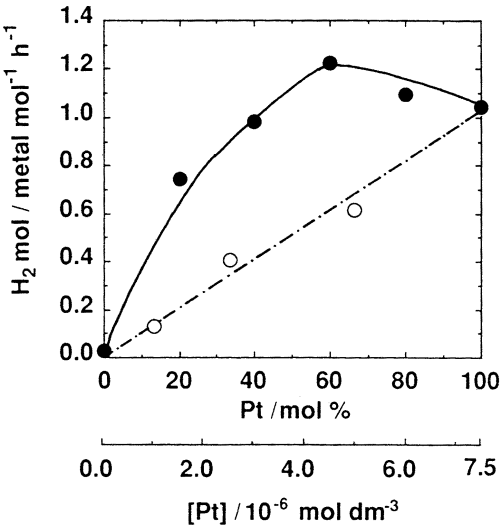

Fig. 45 Catalytic activity of (●) PVP-stabilized Au–Pt bimetallic nanoparticles and (○) PVP-stabilized Pt monometallic nanoparticles at the same concentration for visible light-induced hydrogen generation. (Reprinted with permission from ref. 98. Copyright 1993 Elsevier Science)

electron transfer rate constants (k_e) from methyl viologen cation radical to the metal nanoparticle catalysts. Even when a mixture of Pt and Ru monometallic nanoparticles was used as a catalyst, both k_e and k_{H2} were higher than those of the corresponding monometallic nanoparticles.

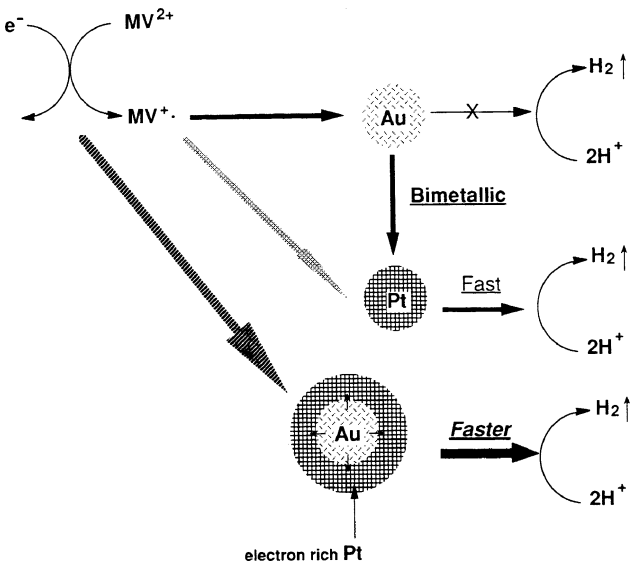

Fig. 46 Schematic diagram of electron transfer and hydrogen generation catalyzed by PVP-stabilized Au–Pt bimetallic nanoparticles. (Reprinted with permission from ref. 98. Copyright 1993 Elsevier Science)

Table 11 Electron transfer constant k_e, hydrogen generation rate constant k_{H2} and average particle diameter d of Pt–Ru bimetallic nanoparticles and monometallic nanoparticles[a]

Metal	k_e/mol^{-1} dm^3 s^{-1}	k_{H2}/s^{-1}	d/nm
Pt–Ru (1 : 1)	830	0.8	2.0
Pt + Ru[b]	650	0.58	—
Ru	580	0.45	2.2
Rh	160	0.15	2.3

[a] Reprinted with permission from ref. 58. Copyright 1997 Elsevier Science. [b] 1 : 1 (mol/mol) physical mixture of Pt and Ru monometallic nanoparticles.

6 Other Aspects

Catalysis is the most widely investigated application of colloidal dispersions of metal nanoparticles at this time. But the properties of metal nanoparticles are now being paid more and more attention by researchers in many fields. For example, non-linear optical properties, especially THG (third harmonic generation), of composites of metal nanoparticles with polymers or glasses have been investigated already, and SERS (surface-enhanced Raman spectroscopy) substrates made of Au or Ag nanoparticles have been proposed. The magnetic properties of colloidal ferromagnetic nanoparticles have also been studied for their application to ferrofluids. Bimetallic and multi-component nanoparticles in particular show very interesting magnetic properties.[147–150] Nanoelectronic devices prepared from careful construction of two- or three-dimensional layers of Au nanoparticles are now a hot topic. Unfortunately we cannot describe these interesting other aspects in this article.

Continued progress in the study of colloidal dispersions of metal nanoparticles, both technological and scientific, will broaden the range of applications of metal nanoparticles with progress in analytic technologies and in controlled synthesis. This progress will again be the center of interest of many researchers.

Acknowledgements

TY thanks Prof. Toyoki Kunitake for his warm hospitality. This work is partly supported by a Grant-in-Aid for Scientific Research on Priority Areas 'New Polymers and Their Nano-Organized Systems' (08246101, NT) and a Grant-in-Aid for the Encouragement of Young Scientists (09740527, TY) from the Ministry of Education, Science, Sports and Culture, Japan.

References

1 H. Hirai and N. Toshima, in *Tailored Metal Catalysts*, ed. Y. Iwasawa, D. Reidel, Dordrecht, 1986, pp. 87–140.
2 G. Schmid, *Polyhedron*, 1988, **7**, 2321.
3 L. N. Lewis, *Chem. Rev.*, 1993, **93**, 2693 .
4 G. Schmid, in *Clusters and Colloids*, VCH, Weinheim, 1994.
5 N. Toshima, *Macromol. Symp.*, 1996, **105**, 111.
6 N. Toshima, in *Fine Particles Science and Technology—From Micro to New Particles*, ed. E. Pelizzetti, Kluewer, Dordrecht, 1996, pp. 371–383.
7 L. Brus, *IEEE J. of Quantum Electron.*, 1986, **22**, 1909.
8 A. Henglein, *Top. Curr. Chem.*, 1988, **143**, 113.
9 A. Henglein, *Chem. Rev.*, 1989, **89**, 1861.
10 H. Weller, *Ber. Bunsenges. Phys. Chem.*, 1991, **95**, 1361.
11 Y.-X. Li and K. J. Klabunde, *Langmuir*, 1991, **7**, 1388.
12 H. Weller, *Angew. Chem.*, 1993, **105**, 43.
13 H. Weller, *Adv. Mater.*, 1993, **5**, 88.
14 G. Schmid, R. Pfeil, R. Boese, F. Bandermann, S. Meyer, G. H. M. Calis and J. W. A. van der Velden, *Chem. Ber.*, 1981, **114**, 3634.
15 G. Schmid and W. Huster, *Z. Naturforsch., Teil B*, 1986, **41**, 1028.
16 K. Meguro, Y. Nakamura, Y. Hayashi, M. Torizuka and K. Esumi, *Bull. Chem. Soc. Jpn.*, 1988, **61**, 347.
17 G. Schmid, B. Morun and J.-O. Malm, *Angew. Chem., Int. Ed. Engl.*, 1989, **28**, 778.
18 H. Bönnemann, W. Brijoux, R. Brinkmann, E. Dinjus, T. Joußen and B. Korall, *Angew. Chem., Int. Ed. Engl.*, 1991, **30**, 1312.
19 J. S. Bradley, J. M. Millar, E. W. Hill, S. Behal, B. Chaudret and A. Duteil, *Faraday Discuss. Chem. Soc.*, 1991, **92**, 255.
20 J. S. Bradley, J. M. Millar, M. Hill and E. W. Hill, *J. Am. Chem. Soc.*, 1991, **113**, 4016.
21 K. Esumi, M. Suzuki, T. Tano, K. Torigoe and K. Meguro, *Colloids Surf.*, 1991, **55**, 9.
22 K. Torigoe and K. Esumi, *Langmuir*, 1992, **8**, 59.
23 I. I. Moissev, M. N. Vargaftik, N. S. Kurnakov, K. I. Zamaraev and D. I. Kochubey, *Mater. Res. Soc. Symp. Proc.*, 1992, **272**, 139.
24 J. S. Bradley, E. W. Hill, S. Behal, C. Klein, B. Chaudret and A. Duteil, *Chem. Mater.*, 1992, **4**, 1234.
25 H. Bönnemann, W. Brijoux, R. Brinkmann, E. Dinjus, R. Fretzen, T. Joußen and B. Korall, *Mater. Res. Soc. Symp. Proc.*, 1992, **272**, 671.
26 M. Brust, M. Walker, D. Bethell, D. J. Schiffrin and R. Whyman, *J. Chem. Soc., Chem. Commun.*, 1994, 801.
27 H. Bönnemann, W. Brijoux, R. Brinkmann, R. Fretzen, T. Joussen, R. Köppler, B. Korall, P. Neiteler and J. Richter, *J. Mol. Catal.*, 1994, **86**, 129.
28 K. Esumi, K. Matsuhisa and K. Torigoe, *Langmuir*, 1995, **11**, 3285.
29 M. Brust, D. Bethell, D. J. Schiffrin and C. J. Kiely, *Adv. Mater.*, 1995, **7**, 795.
30 M. Brust, J. Fink, D. Bethell, D. J. Schiffrin and C. Kiely, *J. Chem. Soc., Chem. Commun.*, 1995, 1655.
31 J. Rothe, J. Pollmann, R. Franke, J. Hormes, H. Bönnemann, W. Brijoux, K. Siepen and J. Richter, *Fresenius' J. Anal. Chem.*, 1996, **355**, 372.
32 T. Yonezawa, M. Sutoh and T. Kunitake, *Chem. Lett.*, 1997, 619.
33 H. Bönnemann and G. A. Braun, *Chem. Eur. J.*, 1997, **3**, 1200.
34 D. de Caro and J. S. Bradley, *Langmuir*, 1997, **13**, 3067.
35 J.-F. You, G. C. Papaefthymiou and R. H. Holm, *J. Am. Chem. Soc.*, 1992, **114**, 2697.
36 H. Gleiter, *Adv. Mater.*, 1992, **4**, 474.
37 D. Ricard, P. Roussignol and C. Flyzanis, *Opt. Lett.*, 1985, **10**, 511.
38 R. F. Marzke, *Catal. Rev.-Sci. Eng.*, 1979, **19**, 43.
39 R. Kubo, *J. Phys. Soc. Jpn.*, 1962, **17**, 975.
40 J. P. Bucher, J. Buttet, J. J. van der Klink, M. Grätzel, E. Newson and T. B. Truong, *Colloids Surf.*, 1989, **36**, 155.
41 J. P. Bucher, J. J. van der Klink and M. Grätzel, *J. Phys. Chem.*, 1990, **94**, 1209.
42 D. van der Putten, H. B. Brom, L. J. de Jongh and G. Schmid, in *Physics and Chemistry of Fine Systems: From Clusters to Crystals*, ed. P. Jena, S. N. Khanna and B. K. Rao, Dordrecht, 1992, vol. II, pp. 1007–1012.
43 Y. Y. Tong, T. Yonezawa, N. Toshima and J. J. van der Klink, *J. Phys. Chem.*, 1996, **100**, 730.
44 L. D. Rampino and F. F. Nord, *J. Am. Chem. Soc.*, 1941, **63**, 3268.
45 L. D. Rampino and F. F. Nord, *J. Am. Chem. Soc.*, 1941, **63**, 2745.
46 K. E. Kavanagh and F. F. Nord, *J. Am. Chem. Soc.*, 1943, **65**, 2121.
47 W. P. Dunworth and F. F. Nord, *J. Am. Chem. Soc.*, 1950, **72**, 4197.
48 H. Hirai, Y. Nakao, N. Toshima and K. Adachi, *Chem. Lett.*, 1976, 905.
49 H. Hirai, Y. Nakao and N. Toshima, *Chem. Lett.*, 1978, 545.
50 N. Toshima, M. Kuriyama, Y. Yamada and H. Hirai, *Chem. Lett.*, 1981, 793.
51 K. Kurihara and J. H. Fendler, *J. Am. Chem. Soc.*, 1983, **105**, 6152.
52 J. S. Bradley, E. Hill, M. E. Leonowicz and H. Witzke, *J. Mol. Catal.*, 1987, **41**, 59.
53 L. N. Lewis, R. J. Uriarte and N. Lewis, *J. Catal.*, 1991, **127**, 67.
54 C. Larpent, F. B.-L. Menn and H. Patin, *J. Mol. Catal.*, 1991, **65**, L35.
55 N. Toshima and T. Takahashi, *Bull. Chem. Soc. Jpn.*, 1992, **65**, 400.
56 G. Schmid, V. Maihack, F. Lantermann and S. Pechel, *J. Chem. Soc., Dalton Trans.*, 1996, 589.
57 G. Schmid, H. West, J.-O. Malm, J.-O. Bovin and C. Grenthe, *Chem. Eur. J.*, 1996, **2**, 1099.
58 N. Toshima and K. Hirakawa, *Appl. Surf. Sci.*, 1997, **121/122**, 534.
59 J. H. Sinfelt, *J. Catal.*, 1973, **29**, 308.
60 J. H. Sinfelt, *Acc. Chem. Res.*, 1987, **20**, 134.
61 N. Toshima, *J. Macromol. Sci., Chem.*, 1990, **A27**, 1225.
62 G. Meitzner, G. H. Via, F. W. Lytle and J. H. Sinfelt, *J. Chem. Phys.*, 1983, **78**, 882.
63 G. Meitzner, G. H. Via, F. W. Lytle and J. H. Sinfelt, *J. Chem. Phys.*, 1983, **78**, 2533.
64 G. Meitzner, G. H. Via, F. W. Lytle and J. H. Sinfelt, *J. Chem. Phys.*, 1985, **83**, 4793.
65 M. Faraday, *Philos. Trans. R. Soc. London*, 1857, **147**, 145.
66 M. Kerker, *J. Colloid Interface Sci.*, 1986, **112**, 302.
67 J. Turkevich and G. Kim, *Science*, 1970, **169**, 873.
68 K. Aika, L. L. Ban, I. Okura, S. Namba and J. Turkevich, *J. Res. Inst. Catal. Hokkaido Univ.*, 1976, **24**, 54.
69 J. Turkevich, P. C. Stevenson and J. Hillier, *Discuss. Faraday. Soc.*, 1951, **11**, 55.
70 H. Hirai, *J. Macromol. Sci., Chem.*, 1979, **A13**, 633.

71 H. Hirai, H. Chawanya and N. Toshima, *Reactive Polym.*, 1985, **3**, 127.
72 B. Zhao and N. Toshima, *Kobunshi Ronbunshu*, 1989, **46**, 551.
73 H. Hirai, Y. Nakao and N. Toshima, *J. Macromol. Sci., Chem.*, 1978, **A12**, 1117.
74 H. Hirai, Y. Nakao and N. Toshima, *J. Macromol. Sci., Chem.*, 1979, **A13**, 727.
75 C. Larpent and H. Patin, *J. Mol. Catal.*, 1988, **44**, 191.
76 G. Schmid and A. Lehnert, *Angew. Chem., Int. Ed. Engl.*, 1989, **28**, 780.
77 J. H. Sinfelt, G. H. Via and F. W. Lytle, *J. Chem. Phys.*, 1980, **72**, 4832.
78 J. H. Sinfelt, G. H. Via and F. W. Lytle, *J. Chem. Phys.*, 1982, **76**, 2779.
79 J. H. Sinfelt, G. H. Via and F. W. Lytle, *J. Chem. Phys.*, 1981, **75**, 5527.
80 R. S. Miner, S. Namba and J. Turkevich, in *Proceedings of the 7th International Congress on Catalysis*, ed. T. Seiyama and K. Tanabe, Kodansha, Tokyo, 1981, p. 160.
81 N. Toshima, M. Harada, T. Yonezawa, K. Kushihashi and K. Asakura, *J. Phys. Chem.*, 1991, **95**, 7448.
82 N. Toshima, K. Kushihashi, T. Yonezawa and H. Hirai, *Chem. Lett.*, 1989, 1769.
83 N. Toshima, T. Yonezawa and K. Kushihashi, *J. Chem. Soc., Faraday Trans.*, 1993, **89**, 2537.
84 D. Richard, J. W. Couves and J. M. Thomas, *Faraday Discuss. Chem. Soc.*, 1991, **92**, 109.
85 B. Zhao and N. Toshima, *Chem. Express*, 1990, **5**, 721.
86 N. Toshima and Y. Wang, *Chem. Lett.*, 1993, 1611.
87 N. Toshima and Y. Wang, *Langmuir*, 1994, **10**, 4574.
88 N. Toshima and Y. Wang, *Adv. Mater.*, 1994, **6**, 245.
89 N. Toshima and P. Lu, *Chem. Lett.*, 1996, 729.
90 J. S. Bradley, E. W. Hill, C. Klein, B. Chaudret and A. Duteil, *Chem. Mater.*, 1993, **5**, 254.
91 K. Esumi, T. Tano, K. Torigoe and K. Meguro, *Chem. Mater.*, 1990, **2**, 564.
92 S. Remita, M. Mostafavi and M. O. Delcourt, *Radiat. Phys. Chem.*, 1996, **47**, 275.
93 A. Henglein, *J. Phys. Chem.*, 1993, **97**, 5457.
94 A. Henglein, P. Mulvaney, A. Holzwarth, T. E. Sosebee and A. Fojtik, *Ber. Bunsenges. Phys. Chem.*, 1992, **96**, 2411.
95 L. Katsikas, M. Gutierrez and A. Henglein, *J. Phys. Chem.*, 1996, **100**, 11203.
96 A. Henglein and C. Brancewicz, *Chem. Mater.*, 1997, **9**, 2164.
97 A. Harriman, *J. Chem. Soc., Chem. Commun.*, 1990, 24.
98 T. Yonezawa and N. Toshima, *J. Mol. Catal.*, 1993, **83**, 167.
99 T. J. Schmidt, M. Noeske, H. A. Gasteiger, R. J. Behm, P. Britz, W. Brijoux and H. Bönnemann, *Langmuir*, 1997, **13**, 2591.
100 L. E. Aleandri, H. Bönnemann, D. J. Johes, J. Richter and J. Roziere, *J. Mater. Chem.*, 1995, **5**, 749.
101 V. M. Deshpande and C. S. Narasimhan, *J. Mol. Catal.*, 1989, **53**, L21.
102 M. Harada, K. Asakura and N. Toshima, *J. Phys. Chem.*, 1993, **97**, 5103.
103 G. Schmid, A. Lehnert, J.-O. Malm and J.-O. Bovin, *Angew. Chem., Int. Ed. Engl.*, 1991, **30**, 874.
104 J. H. Michel and J. T. Schwartz, *Stud. Surf. Sci. Catal.*, 1987, **31**, 669.
105 Y. Degani and I. Willner, *J. Chem. Soc., Perkin Trans. 2*, 1986, 37.
106 Y. Wang and N. Toshima, *J. Phys. Chem. B*, 1997, **101**, 5301.
107 K. Torigoe and K. Esumi, *Langmuir*, 1993, **9**, 1664.
108 K. Torigoe, Y. Nakajima and K. Esumi, *J. Phys. Chem.*, 1993, **97**, 8304.
109 M. T. Reetz and W. Helbig, *J. Am. Chem. Soc.*, 1994, **116**, 7401.
110 M. T. Reetz, W. Helbig and S. A. Quaiser, *Chem. Mater.*, 1995, **7**, 2227.
111 M. T. Reetz and S. A. Quaiser, *Angew. Chem., Int. Ed. Engl.*, 1995, **34**, 2240.
112 J. S. Bradley, in *Clusters and Colloids*, ed. G. Schmid, VCH, Weinheim, 1994, pp. 459–544.
113 D. G. Duff, A. C. Curtis, P. P. Edwards, D. A. Jefferson, B. F. G. Johnson and D. E. Logan, *J. Chem. Soc., Chem. Commun.*, 1987, 1264.
114 A. C. Curtis, D. G. Duff, P. P. Edwards, D. A. Jefferson, B. F. G. Johnson, A. I. Kirkland and A. S. Wallace, *J. Phys. Chem.*, 1988, **92**, 2270.
115 M. Harada, K. Asakura and N. Toshima, *J. Phys. Chem.*, 1994, **98**, 2653.
116 N. Toshima, T. Yonezawa, M. Harada, K. Asakura and Y. Iwasawa, *Chem. Lett.*, 1990, 815.
117 T. Yonezawa and N. Toshima, *J. Chem. Soc., Faraday Trans.*, 1995, **91**, 4111.
118 J. S. Bradley, G. H. Via, L. Bonneviot and E. W. Hill, *Chem. Mater.*, 1996, **8**, 1895.
119 L. Zhu, K. S. Liang, B. Zhang, J. S. Bradley and A. E. Depristo, *J. Catal.*, 1998, **167**, 412.
120 Y. Wang and H. Liu, *Polym. Bull.*, 1991, **25**, 139.
121 K. C. Grabar, K. J. Allison, B. E. Baker, R. M. Bright, K. R. Brown, R. G. Freeman, A. P. Fox, C. D. Keating, M. D. Musick and M. J. Natan, *Langmuir*, 1996, **12**, 2353.
122 K. C. Grabar, K. R. Brown, C. D. Keating, S. J. Stranick, S.-L. Tang and M. J. Natan, *Anal. Chem.*, 1997, **69**, 471.
123 J. Schmitt, G. Decher, W. J. Dressick, S. L. Brandow, R. E. Geer, R. Shashidhar and J. M. Calvert, *Adv. Mater.*, 1997, **9**, 61.
124 T. Yonezawa, S. Onoue and T. Kunitake, *Adv. Mater.*, 1998, **10**, 414.
125 D. G. Duff, P. P. Edwards, J. Evans, J. T. Gauntlett, D. A. Jefferson, B. F. G. Johnson, A. I. Kirkland and D. J. Smith, *Angew. Chem., Int. Ed. Engl.*, 1989, **28**, 590.
126 U. Kolb, S. A. Quaiser, M. Winter and M. T. Reetz, *Chem. Mater.*, 1996, **8**, 1889.
127 A. Traverse, *New J. Chem.*, 1998, **22**, 677.
128 R. Touroude, P. Girard, G. Maire, J. Kizling, M. Boutonnet-Kizling and P. Stenius, *Colloids Surf.*, 1992, **67**, 9.
129 M. Harada, K. Asakura, Y. Ueki and N. Toshima, *J. Phys. Chem.*, 1992, **96**, 9730.
130 J. P. Bucher and J. J. van der Klink, *Phys. Rev. B*, 1988, **38**, 11038.
131 Y. Y. Tong, G. A. Martin and J. J. van der Klink, *J. Phys. D*, 1994, **6**, L533.
132 J. J. van der Klink, in *Physics and Chemistry of Fine Systems: From Clusters to Crystals*, ed. P. Jena, S. N. Khanna and B. K. Rao, Dordrecht, 1992, vol. I, pp. 537–547.
133 T. Yonezawa, Y. Gotoh and N. Toshima, *Chem. Express*, 1993, **8**, 545.
134 T. Yonezawa, Y. Gotoh and N. Toshima, *Reactive Polym.*, 1994, **23**, 43.
135 T. Yonezawa, T. Tominaga and D. Richard, *J. Chem. Soc., Dalton Trans.*, 1996, 1996, 783.
136 L. J. de Jongh, J. Baak, H. B. Brom and D. van der Putten, in *Physics and Chemistry of Fine Systems: From Clusters to Crystals*, ed. P. Jena, S. N. Khanna and B. K. Rao, Dordrecht, 1992, vol. II, pp. 839–851.
137 N. Toshima, M. Harada, Y. Yamazaki and K. Asakura, *J. Phys. Chem.*, 1992, **96**, 9927.
138 N. Toshima and T. Yonezawa, *Makromol. Chem., Macromol. Symp.*, 1992, **59**, 281.
139 K. Asakura, Y. Yamazaki, H. Kuroda, M. Harada and N. Toshima, *Jpn. J. Appl. Phys.*, 1993, **32** (Suppl. 32-2), 448.
140 R. Ramaraj, A. Kira and M. Kaneko, *Angew. Chem., Int. Ed. Engl.*, 1986, **25**, 825.
141 T. Ohno, S. Saito, K. Fujihara and M. Matsumura, *Bull. Chem. Soc. Jpn.*, 1996, **69**, 3059.
142 J.-M. Lehn and J.-P. Sauvage, *New J. Chem.*, 1978, **1**, 449.
143 N. Toshima, T. Takahashi and H. Hirai, *Chem. Lett.*, 1986, 35.
144 Y. Nakato, H. Yano, S. Nishiura, T. Ueda and H. Tsubomura, *J. Electroanal. Chem.*, 1987, **228**, 97.
145 N. Toshima, T. Takahashi and H. Hirai, *Chem. Lett.*, 1987, 1031.
146 N. Toshima, T. Takahashi and H. Hirai, *J. Macromol. Sci., Chem.*, 1988, **A25**, 669.
147 K. J. Klabunde, *Free Atoms, Clusters, and Nanoscale Particles*, Academic Press, San Diego, 1994.
148 S. Utamapanya, K. J. Klabunde and J.R. Schlup, *Chem. Mater.*, 1991, **3**, 175.
149 T. Boronina, K. J. Klabunde and G.l Sergeev, *Environ. Sci. Tech.*, 1996, **30**, 3645.
150 O. Koper, I. Lagadic and K. J. Klabunde, *Chem. Mater.*, 1997, **9**, 838.

Received in Mülheim an der Ruhr, Germany, 22*nd July* 1998; *Paper* 8/05753B